haematologica
Journal of The Ferrata Storti Foundation

Monomorphic epitheliotropic intestinal T-cell lymphoma comprises morphologic and genomic heterogeneity impacting outcome

by Luis Veloza, Doriane Cavalieri, Edoardo Missiaglia, Albane Ledoux-Pilon, Bettina Bisig, Bruno Pereira, Christophe Bonnet, Elsa Poullot, Leticia Quintanilla-Martinez, Romain Dubois, Francisco Llamas-Gutierrez, Céline Bossard, Roland De Wind, Fanny Drieux, Juliette Fontaine, Marie Parrens, Jeremy Sandrini, Virginie Fataccioli, Marie-Hélène Delfau-Larue, Adrien Daniel, Faustine Lhomme, Lauriane Clément-Filliatre, François Lemonnier, Anne Cairoli, Pierre Morel, Sylvie Glaisner, Bertrand Joly, Abderrazak El Yamani, Kamel Laribi, Emmanuel Bachy, Reiner Siebert, David Vallois, Philippe Gaulard, Olivier Tournilhac, and Laurence de Leval

Received: April 12, 2022.
Accepted: June 9, 2022.

Citation: Luis Veloza, Doriane Cavalieri, Edoardo Missiaglia, Albane Ledoux-Pilon, Bettina Bisig, Bruno Pereira, Christophe Bonnet, Elsa Poullot, Leticia Quintanilla-Martinez, Romain Dubois, Francisco Llamas-Gutierrez, Céline Bossard, Roland De Wind, Fanny Drieux, Juliette Fontaine, Marie Parrens, Jeremy Sandrini, Virginie Fataccioli, Marie-Hélène Delfau-Larue, Adrien Daniel, Faustine Lhomme, Lauriane Clément-Filliatre, François Lemonnier, Anne Cairoli, Pierre Morel, Sylvie Glaisner, Bertrand Joly, Abderrazak El Yamani, Kamel Laribi, Emmanuel Bachy, Reiner Siebert, David Vallois, Philippe Gaulard, Olivier Tournilhac, and Laurence de Leval. Monomorphic epitheliotropic intestinal T-cell lymphoma comprises morphologic and genomic heterogeneity impacting outcome.
Haematologica. 2022 June 16. doi: 10.3324/haematol.2022.281226. [Epub ahead of print]

Monomorphic epitheliotropic intestinal T-cell lymphoma comprises morphologic and genomic heterogeneity impacting outcome

*Luis Veloza[1], *Doriane Cavalieri[2], Edoardo Missiaglia[1], Albane Ledoux-Pilon[3], Bettina Bisig[1], Bruno Pereira[4], Christophe Bonnet[5], Elsa Poullot[6], Leticia Quintanilla-Martinez[7], Romain Dubois[8], Francisco Llamas-Gutierrez[9], Céline Bossard[10], Roland De Wind[11], Fanny Drieux[12], Juliette Fontaine[13], Marie Parrens[14], Jeremy Sandrini[15], Virginie Fataccioli[6,16], Marie-Hélène Delfau-Larue[16,17], Adrien Daniel[18], Faustine Lhomme[19], Lauriane Clément-Filliatre[20], François Lemonnier[16,21], Anne Cairoli[22], Pierre Morel[23], Sylvie Glaisner[24], Bertrand Joly[25], Abderrazak El Yamani[26], Kamel Laribi[27], Emmanuel Bachy[28], Reiner Siebert[29], David Vallois[1], #Philippe Gaulard[6,16], #Olivier Tournilhac[2], #Laurence de Leval[1]

* Co-first authors #co-last authors

[1] Institute of Pathology, Department of Laboratory Medicine and Pathology, Lausanne University Hospital and Lausanne University, Lausanne, Switzerland

[2] Department of Hematology, University Hospital of Clermont-Ferrand, Clermont-Ferrand, France

[3] Department of Pathology, University Hospital of Clermont-Ferrand, Clermont-Ferrand, France

[4] Clinical Research Direction, University Hospital of Clermont-Ferrand, Clermont-Ferrand, France

[5] Department of Hematology, University Hospital Sart Tilman, Liège, Belgium

[6] AP-HP, Henri Mondor Hospital, Pathology Department, F-94010 Créteil, France

[7] Institute of Pathology, University Hospital Tübingen, Eberhard Karls University of Tübingen, Tübingen, Germany

[8] Department of Pathology, University Hospital of Lille, Lille, France

[9] Department of Pathology, University Centre Hospital, Rennes, France

[10] Department of Pathology, CHU de Nantes, France

[11] Department of Pathology, Institute Jules Bordet, Bruxelles, Belgique

[12] Centre Henri Becquerel, Service of Anatomical and Cytological Pathology, Centre Henri Becquerel Rouen, France, Rouen, France

[13] Multisite pathology Institute, Hôpital Lyon Sud, Hospices Civils de Lyon, Pierre Bénite, France

[14] Department of Pathology, CHU de Bordeaux, University of Bordeaux, Bordeaux, France

[15] Department of Pathology, Le Mans Hospital Center, 72000 Le Mans, France

[16] University Paris Est Créteil, INSERM, IMRB, F-94010 Créteil, France

[17] Department of Immunobiology and Inserm U955, Henri Mondor University Hospital, Créteil, France

[18] Department of Hematology, University Hospital of Lille, Lille, France

[19] Department of Hematology, University Hospital of Rennes, Hospital Pontchaillou, Rennes, France

[20] Department of Oncology, Louis Pasteur clinic, Essey-Lès-Nancy, France

[21] AP-HP, Henri Mondor Hospital, Lymphoid malignancies unit, F-94010 Créteil, France

[22] Service of Hematology, Department of Oncology, Lausanne University, Hospital and Lausanne University, Lausanne, Switzerland

[23] Department of Hematology, Hospital of Lens, Lens, France and Department of Hematology, University Hospital of Amiens, Amiens, France

[24] Department of Hematology, Institute Curie, Hospital Rene Huguenin, Saint-Cloud, France

[25] Department of Hematology, Sud-Francilien Hospital Centre, Corbeil-Essonnes, France

[26] Department of Hematology, Hospital Centre of Blois, Blois, France

[27] Department of Hematology, Hospital Centre Le Mans, Le Mans, France

[28] Department of Hematology, Centre Hospitalier Lyon Sud & Inserm U1111, Pierre Bénite, France

[29] Institute of Human Genetics, Ulm University and Ulm University Medical Center, Ulm, Germany

Running title: MEITL: genetic heterogeneity impacting outcome

Corresponding author: Laurence de Leval, MD PhD, Institute of Pathology, Lausanne University Hospital and Lausanne University, Lausanne, Switzerland. Laurence.deleval@chuv.ch.

Data sharing statement: Original data and protocols will be available to other investigators by request to corresponding author.

Word counts main text: 4009

Word count abstract: 256

Figure count: 5

Table count: 3

Supplementary files: 1

Acknowledgments:

The work developed at the Institute of Pathology of Lausanne, was supported by the histopathology, immunopathology and molecular pathology facilities, and the digital pathology platform of the Institute. The authors would like to thank Dr Nathalie Piazzon and Mr Jean-Daniel Roman for assistance with data management, Mrs Catherine Chapuis for technical assistance, Dr Justine Bouilly and Dr Audrey Letourneau for analysis and interpretation of TDS data and Mrs Cloé Bregnard and Mónica Esteves De Azevedo for performing the FISH studies. They also thank Dr Amedeo Sciarra for his contribution to data coding, Dr Adamantia Kapopoulou and Mr Vimel Rattina for their contribution in whole exome analysis and Mr Venkatesh Kacherla in the preparation of Figure 4 panels. The authors are indebted to Mrs Julien Marquis and Johann Weber from the Lausanne Genomic Technologies

Facility, Center forIntegrative Genomics of Lausanne University where whole exome sequencing was performed.

The authors would like to thank Drs Patrick Bruandet and Jacques Akpo-Allavo (Service de Pathologie CH Blois), Drs Florence Bloget and Damienne Declerck (Medipath, Avon), Drs François Lamarche and Caroline Ghighi (ACP, Abbeville), Drs Pierre Boyer and Jean Kapfer (CAP Orléans), Prof. Luc Xerri (Service de Pathologie, IPC Marseille) and Dr Thérèse Rousset (Service de Pathologie, CHU Montpellier) for providing tumor material. Dr Olivier Dubroeucq (Institut Jean Godinot, Reims), Dr Bruno Villemagne (CHD Vendée), Dr Emmanuelle Tchernonog (CHU de Montpellier), Dr Sara Burcheri (CH Perpignan), Dr Sophie Rigaudeau (CH de Versailles), Pr Emmanuel Gyan (CHU de Tours), Dr Julie Abraham (CHU de Limoges), Dr Emmanuel Fleck (CH de La Rochelle), Dr Eric Dupont (CH d'Agen), Dr Jean Galtier (CHU de Bordeaux), Dr Thibault Brotelle (CH d'Avignon), Pr Gandhi Damaj (CHU de Caen), Dr Serge Bologna (Centre d'oncologie de Gentilly), Dr Clémentine Sarkozy (Institut Gustave Roussy), Dr Marion Loirat (CH de Saint-Nazaire), Dr Valentin Letailleur (CHU de Nantes), Dr Pierre Englert (Hôpital Erasme, Bruxelles), Romane Muletier (CHU de Clermont-Ferrand), Dr Shota Tsiklauri (CH d'Aubenas), Dr Bernard Drenou (GHR Mulhouse Sud-Alsace), Dr Florian Bouclet (Centre Henri Becquerel, Rouen), Dr Robin Noël (Institut Paoli Calmettes, Marseille), Dr Patrick Mboungou (CH de Boulogne-Sur-Mer), Dr Abdallah Maakaroun (CH de Bourges) and the Hospitals of Dieppe, Mont-de-Marsan, Sud Seine-et-Marne, the Clinique du Saint-Cœur, the Clinique de l'Archette, the Polyclinique du Ternois are acknowledged for providing clinical follow up.

This work was supported by the grants KLS-4293-08-2017-R to LDL of the Swiss Cancer Ligue and SNSF – 31BL30_172718 to LDL of the Patholink and the Swiss National Science Foundation.

It was presented in part at the 16th International Conference on Malignant Lymphoma (Lugano, 2021).

Authorship contribution

LV reviewed morphological data, analyzed data, and wrote the manuscript. DC reviewed and interpreted clinical data and wrote the manuscript. EM analyzed and interpreted sequencing data and wrote the manuscript. BP analyzed data and supervised the statistical analysis. BB supervised FISH and TDS analyses. CB, AD, FL, LCF, FL, AC, PM, SG, BJ, AEY, KL, EB reviewed and interpreted clinical data. ALP, EP, LQM, RB, FRG, CB, RDW, FD, JF, MP, JS performed morphological diagnoses. MHDL contributed with molecular data of cases. VF supported material and data acquisition and collected data. RS reviewed and analyzed genomic data. DV performed research and analyzed the data. PG performed morphological diagnoses, designed research, and analyzed data. OT reviewed and interpreted clinical data, designed research, and wrote the manuscript. LdL performed morphological diagnoses, designed research, obtained funding, analyzed data, and wrote the manuscript.

Conflict-of-interest disclosure

The authors have no conflict of interest to disclose.

Abstract

Monomorphic epitheliotropic intestinal T-cell lymphoma (MEITL) is a rare aggressive T-cell lymphoma most reported in Asia. We performed a comprehensive clinical, pathological and genomic study of 71 European MEITL patients (36 males; 35 females, median age 67 years). The majority presented with gastrointestinal involvement and had emergency surgery, and 40% had stage IV disease. The tumors were morphologically classified into two groups: typical (58%) and atypical (i.e. non-monomorphic or with necrosis, angiotropism or starry-sky pattern) (42%), sharing a homogeneous immunophenotypic profile (CD3+ (98%) CD4- (94%) CD5- (97%) CD7+ (97%) CD8+ (90%) CD56+ (86%) CD103+ (80%) cytotoxic marker+ (98%)) with more frequent expression of TCRgd (50%) than TCRab (32%). MYC expression (30% of cases) partly reflecting *MYC* gene locus alterations, correlated with non-monomorphic cytology. Almost all cases (97%) harbored deleterious mutation(s) and/or deletion of the *SETD2* gene and 90% had defective H3K36 trimethylation. Other frequently mutated genes were *STAT5B* (57%), *JAK3* (50%), *TP53* (35%) *JAK1* (12.5%), *BCOR* and *ATM* (11%). Both *TP53* mutations and MYC expression correlated with atypical morphology. The median overall survival (OS) of 63 patients (43/63 only received chemotherapy after initial surgery) was 7.8 months. Multivariate analysis found a strong negative impact on outcome of MYC expression, *TP53* mutation, *STAT5B* mutation and poor performance status while aberrant B-cell marker expression (20% of cases) correlated with better survival. In conclusion, MEITL is an aggressive disease with resistance to conventional therapy, predominantly characterized by driver gene alterations deregulating histone methylation and JAK/STAT signalling and encompasses genetic and morphologic variants associated with very high clinical risk.

Introduction

Monomorphic Epitheliotropic Intestinal T-cell Lymphoma (MEITL), formerly considered as a variant (type II) of enteropathy-associated T-cell lymphoma (EATL), is now recognized a separate entity based on distinct clinicopathological and epidemiological features, unrelated to celiac disease (CD)[1]. MEITL and EATL are both rare accounting together for less than 5% of peripheral T-cell lymphomas[2,3]. Many published series describe hybrid cohorts comprising MEITL and EATL[4-8]. In Western countries, the incidence of MEITL is even lower than the incidence of EATL. In contrast, in Asia where CD is essentially not existing, MEITL is the most common type of primary gastrointestinal T-cell lymphoma[9-15].

As opposed to EATL, MEITL is defined as a tumor composed of monomorphic medium-sized cells, with round nuclei and a rim of pale cytoplasm, typically showing striking infiltration of intestinal epithelium and lacking necrosis or significant inflammation[1,16]. EATL and MEITL have in common an activated cytotoxic T-cell immunophenotype while distinctive MEITL features include expression of CD8 and CD56, negativity for CD30 and occasional CD20 expression[4-6, 8,10-14,17,18].

The mutational landscape of MEITL encompasses frequent activating mutations of the JAK/STAT signaling pathway mainly affecting *STAT5B* (33-65%), *JAK3* (33-67%) and *JAK1* (5-44%)[7,18-23]. Moreover, activating hotspot mutations in the *GNAI2* gene coding for guanine nucleotide-binding protein G(i), alpha-2 subunit have been reported in 21% of the cases in a study from Singapore[20]. We reported highly recurrent (>90%) deleterious alterations in the *SETD2* gene coding for SET Domain Containing 2, a histone lysine methyltransferase, which has been variably confirmed in subsequent studies[7,18,20,23].

MEITL usually presents as a small bowel tumor often manifesting by perforation or obstruction, abdominal pain and weight loss. The disease follows an aggressive course with a median OS usually of less than one year (range 6.5 - 14 months)[6,8,9,13,18,24]. No robust prognostic or predictive biomarkers have been described to date.

Here, we studied a large series of 71 MEITL cases from Western Europe, performed histopathological assessment supplemented by extensive immunophenotyping, targeted FISH studies, and mutational analysis of a selected 27-gene panel in 65 cases. We present a comprehensive analysis integrating the pathological and molecular features and their correlation to clinical outcome.

Methods

Patients and samples

Seventy-one patients diagnosed with MEITL between 2005 and 2021 according to 2008 or 2017 WHO classifications[1,16] (69 diagnostic and 2 relapse samples, all routinely processed formalin-fixed paraffin embedding (FFPE) tissues) were collected through the Tenomic Consortium of the Lymphoma Study Association (LYSA)[25] (n=65) and the University Hospital of Tübingen, Germany (n=6). Twenty-nine cases were included in a previous study[7]. The clinical history and imaging studies were collected from the patients' files by the treating physicians. The study was approved by the Commission cantonale d'éthique de la recherche sur l'être humain (CER-VD, protocol 382/14), the Comité de Protection des Personnes-Ile-de-France IX (CPP08/009), and the Ethical Committee of the University of Tübingen (105/2013BO2) in accordance with the Declaration of Helsinki.

Histology, immunohistochemistry and FISH

Diagnostic slides were reviewed. Additional immunostains and EBER *in situ* hybridization for detection of the Epstein-Barr virus (EBV) were performed using standard protocols (**Supplemental methods** and **Table S1**). Immunostainings were evaluated semi-quantitatively by at least two pathologists. For most markers a five-tier scale was used (<5%, 5-25%, 26-50%, 51-75%, 76-100%), and a threshold of 5% was considered for positive score. Ki-67, MYC and p53 staining were scored into quartiles (<25%, 26-50%, 51-75%, 76-100%). For fluorescence in situ hybridization (FISH) evaluation of the *SETD2* and *MYC* gene loci we used a homemade *SETD2* probe[7] and the commercial LSI *MYC* Dual Color Break Apart probe (8q24) (Abbott Molecular, Des Plaines, IL, USA) (**Supplemental methods**)**.** Chromogenic slides were digitalized using a NanoZoomer S60 Digital slide scanner (Hamamatsu Photonics, Japan) at 40x magnification and evaluated using a digital image viewer system (TM-Microscopy, Telemis, Belgium). Morphology, IHC and FISH results were recorded in a coded dataset (**Supplemental Figure S1**).

Deep sequencing and mutation analysis

Sixty-five cases were examined by DNA sequencing (NGS). Data were generated by WES in 34 cases, including 14 previously reported[7], and by targeted deep sequencing (TDS) using a customized 27-gene panel relevant to T-cell lymphoma biology in 29 cases, or a 9-gene panel TDS assay[7,26] in two cases. For WES, libraries from tumor and matched non-tumor DNA, both extracted from FFPE tissues, were paired-end sequenced on a HiSeq 4000 instrument (Illumina, San Diego, CA). For TDS, libraries of tumor DNA prepared with the KAPA HyperPlus kit (Roche, Pleasanton, CA) were target enriched by capture prior to sequencing on a MiSeq system (Illumina). After demultiplexing, alignment and duplicate removal, single

nucleotide and indel variant calling was performed using three caller algorithms VarScan (v2.4.4) and MuTect2 algorithm (GATK v4.1). For WES set, the variant call was restricted to the 27 genes of the TDS panel plus *GNAI2*.

Statistical methods

Fisher's exact or χ^2 tests were used to determine associations between morphological, immunophenotypical and genetic characteristics. Estimates of overall survival were constructed using the Kaplan-Meier method. Cox proportional hazards regression model was used to investigate associated prognostic factors in univariate and multivariable analysis. To ensure the robustness of our results, the final model was validated by a two-step bootstrapping process. Results were expressed as hazard-ratio (HR) and 95% confidence interval. Statistical analysis was performed using Stata software (version 15, StataCorp LP, College Station, US). The tests were two-sided, with a type I error set at 5%. When appropriate, a correction of the type I error was applied to take into account multiple comparisons.

Results

Patients' characteristics

The 36 male and 35 female patients had a median age of 67 years (range 29-91 years). Baseline clinical and biological features of 63 patients are presented in **Table 1** and **Supplemental Tables S2** and **S3**. All had gastrointestinal involvement, most often restricted to the small intestine (n=46/63, 73%) and most patients (52/61, 85%) presented with acute symptoms, mainly related to intestinal perforation and/or obstruction. According to the Lugano staging system: 33% (n=20) had only GI involvement (stage I), 27% (n=16) had local or abdominal lymph nodes (stage II),

40% (n=24) were stage IV with supradiaphragmatic lymph nodes or extradigestive/extranodal involvement, most commonly pleuro-pulmonary (n= 7), or hepatic (n=4). Hypermetabolic lesion(s) with maximal Standardized Uptake Values (SUV) ranging from 8 to 30 were reported in 27/28 patients.

Histopathology

The main histopathological features are summarized in **Figure 1**. The size of intestinal tumors ranged from 1.7 to 20 cm (median 6 cm). Except for one case with mainly mucosal involvement, 61/62 (98%) surgical specimens comprised a frequently ulcerated transmural central zone, perforated in 44/58 cases (76%), and showed lateral tumor extension predominant in the mucosa (peripheral zone)[10,17] in 40/46 (87%) evaluable cases (**Figure 2A**). Most intestinal cases (48/54, 89%) showed tumor epitheliotropism (**Figure 1**, **2B, 2D** and **2E)**. Morphology of other tumor locations with epitheliotropism in non-intestinal sites are illustrated in **Supplemental Figure S2A-2H** and **Figure 3J-3L.**

Most cases (53/71, 75%) showed classical monomorphic cytology, i.e. round and small/medium-sized tumor cells with little variation in nuclear size, slightly dispersed chromatin, inconspicuous nucleoli, and ample pale cytoplasm (**Figure 2B-C**). However, a significant proportion of cases (18/71, 25%) showed either significant cellular pleomorphism, larger cell size, vesicular chromatin and/or prominent nucleoli (**Figure 3A** and **3O** and **Supplemental Figure S3D-3F**)**.** A peculiar, atypical case (#66) had two distinct monomorphic and non-monomorphic components (**Supplemental Figure S4**). Except for two non-monomorphic cases, which had abundant eosinophils and prominent plasma cells, all cases presented very few

inflammatory cells. Mitoses were easily identified in most cases. While mitoses were easily identified in most cases, a small subset (7/71 cases, 10%), appeared as high-grade neoplasms with a “starry-sky” pattern or abundant apoptotic debris (**Figure 3** and **Supplemental Figure S3A-C**). Other unusual features were seen in a subset of cases: coagulative necrosis distinct from surface ulceration in 9 cases (**Figure 3N**)**,** or focal or prominent angiotropism or angioinvasion of medium to large-sized blood vessels in 18 cases (**Figure 3B** and **3M**), which were frequent among non-monomorphic cases (**Supplemental Table S4**). Overall, we distinguished two morphological groups of cases: typical tumors (n=41, 58%) and atypical tumors (n=30, 42%) featuring one or more atypical histological characteristic(s) (**Figure 1** and **Table 2**).

Immunophenotype and EBV status

The immunophenotypic profiles are shown in **Figure 1** and summarized in **Table 2**. Most cases had homogeneous and strong expression of CD3 (70/71, 99%) and CD7 (63/65, 97%). CD2 was positive in 32/66 cases (48%). Only 2/70 (3%) cases were CD5-positive. CD8 and CD56 were usually widely expressed, but with heterogeneous staining intensity. Most cases (55/71, 77%) were positive for both CD56 and CD8, 9/71 (13%) were CD8+ CD56-, 6/71 (8%) were CD8- CD56+, and one case CD8- CD56-. Four cases, all CD8+ CD56+, were strongly CD4-positive. CD30 was negative in all cases (63/64, 98%), except in occasional large, atypical cells in case #66 (**Supplemental Figure S4**). PD1 was negative in 20/20 tested cases. Most cases strongly expressed TIA1 in most tumor cells (65/68, 96%) (**Figure 3G**); but immunostains for granzyme B and perforin, positive in 50/66 cases (76%) and 39/62 cases (63%) respectively, were frequently weaker with often <50% positive tumor

cells. Overall, 59/68 (87%) cases had an activated cytotoxic profile**,** 11 cases expressed TIA1 only and one case was negative for the three cytotoxic markers.

Half of cases (32/64, 50%) expressed TCRγ and/or TCRδ (TCRγδ+), and 21/65 (32%) cases were positive for TCRβ (TCRαβ+). Sixty-two cases with contributory results for both TCR isoforms were classified as single positive for TCRγδ (43%) (**Figure 3C**) or TCRαβ (24%) (**Figure 2J**), TCR silent (24%), or double positive (9%) (**Supplemental Figure S3G-3I**).

Fifty-two out of 65 cases (80%) were CD103-positive. Apart from few cases homogeneously and intensely CD103-positive, in most cases a gradient of staining was observed from more intense and extensive in the intramucosal portion to weaker or negative in the deeper infiltrative part (**Figure 2K-2L**).

Coexpression of CD20, usually by <50% of the tumor cells and weaker than in normal B cells, was observed in 12/67 (18%) cases. Four out of 51 (8%) cases were CD79a+. Two cases coexpressed CD20 and CD79a (**Supplemental Figure S3A-3C**), but lacked PAX5 and were positive for CD8, CD56 and cytotoxic markers. All 24 tested cases for PAX5 were negative. In total, 14/67 (20%) were B-cell marker-positive.

Ki-67 proliferation index was >75% in most cases (38/68, 56%) (**Figure 1** and **3H**). All 68 cases tested for EBV by EBER-ISH were negative, and one case showed scattered reactive small (<1%) EBV-positive cells.

There were no significant differences in the immunophenotypic profiles of atypical and typical cases (**Table 2** and **Supplemental Table S4**).

SETD2 gene alterations and defective H3K36me3 trimethylation

By NGS analysis (**Supplemental Table S5** and **Figure 4A**), we found a very high prevalence of *SETD2* mutations in 59/65 cases (91%), with two mutations in 29/59 cases (49%) and 3 mutations in one case (#59) (**Figure 4B**). Of the 88 *SETD2* mutations identified, 62 (27 nonsense, 26 frameshift and 9 splice-sites) were likely generating a truncated non-functional protein and were distributed throughout the whole gene domains. Moreover, most of the 24 missense mutations clustered within the SET domain of the SETD2 protein or its proximity. Notably, the 24 cases analysed by both WES and TDS (this latter only on the tumour component) showed complete overlap, indicating absence of germline variants in this subset of patients. Heterozygous deletions of *SETD2* were observed in 9/57 (16%) cases evaluated by FISH, of which 6 had one or two concurrent *SETD2* mutation(s), and 3 were *SETD2* wild-type (**Figure 3D**). Overall, of 54 cases with complete NGS and FISH results for *SETD2*, 23 had one mutation or deletion, 29 had two or more alterations and only 2 (4%) had no detectable alteration. These latter two cases (#6 and #49) were non-monomorphic, with a characteristic CD8+, CD56+, TCRγδ+ cytotoxic phenotype, and harbored other mutations in the JAK/STAT pathway.

Immunohistochemistry was performed to assess the SETD2–H3K36me2–H3K36me3 axis at the protein level (**Figure 1**). Defective expression of SETD2 or H3K36me3 (IHC scores ≤ 6) were observed in 47/55 cases (85%) and 60/66 cases (91%), respectively. The correlation between *SETD2* gene alterations and SETD2 protein expression (**Figure 1**) was concordant in 43/50 cases (86%); six cases with *SETD2* gene alteration had preserved SETD2 expression, and one case had defective protein expression and no detectable gene alteration. H3K36me3 IHC results were concordant with the *SETD2* status, in 60/63 cases (95%) i.e. 58 cases

had defective H3K36me3 trimethylation (H3K36me3 score ≤ 6) and altered *SETD2*, and two cases with high H3K36me3 scores had no detected *SETD2* alteration. Only three cases, two with monoallelic alteration and one with double mutations of *SEDT2,* had high H3K36me3 scores. Thus, H3K36me3 IHC as a surrogate to identifying *SETD2* gene alterations was highly sensitive (95%), and 100% specific (K=0.55, 95% CI (0.11-0.99) p<0.015) (**Figure 3E-3F** and **Supplemental Figure S5**)

Mutations in other genes

The second most frequently mutated gene was *STAT5B* featuring alterations in 37/65 cases (57%) (**Figure 4**). *STAT5B* mutations were all missense, single (n=31) or double (n=6). Most mutations (70%) occurred in the SH2 domain, including the hotspot N642H activating mutation in 21 patients[7]. *JAK3* mutations found in 32/64 cases (50%) included several activating variants clustered in the pseudokinase domain (such as A573V, M511I, R657W, K563_566del, P676R), and were single (n=29) or double (n=2). *JAK1* mutations were identified in a smaller proportion of cases (8/64, 12%). Mutations in *STAT5B, JAK3* and *JAK1* were not mutually exclusive. In all, 54/64 cases (84%) had mutations in at least one gene of the JAK/STAT pathway. Notably, *STAT5B* mutations showed significantly higher allele frequencies than *JAK3* and *SETD2* mutations, likely due to co-occurring loss-of-heterozygosity (LOH) or allelic imbalance events (**Supplemental Figure S6**).

TP53 mutations were identified in 22/63 (35%) cases and, similar to *STAT5B* mutations, were also associated with a high-allele frequencies due to copy number losses or copy number neutral LOH events (**Supplemental Figure S6**). Remarkably, *TP53* mutations occurred mostly among the atypical group (adj. p 0.01, Fisher's

exact test) (**Table 2**) and correlated with abnormal p53 IHC pattern – either overexpression (>50%) or uncommonly completely negative staining in 2 cases (adj. p <0.001, Fisher's exact test) (**Figure 1, 3I** and **Supplemental Table S4**)**.**

Mutations in *BCOR* and *ATM* were found in 11% of cases each. Three of 34 cases (9%) carried somatic mutations in the *GNAI2* gene; two in codon R179 previously described[20], and one p.T182I mutation.

MYC status

Twelve of 60 cases subjected to FISH (20%) had *MYC* gene locus alterations, i.e. copy gains in eight and breaks (rearrangements) in four cases. None of the cases with *MYC* copy gain was hyperploid (**Supplemental methods**). Ten of the 12 cases with *MYC* gene alterations had >25% MYC-protein positive tumor cells by immunohistochemistry. Overall, MYC expression of detected in 18/54 cases (33%), more frequently among non-monomorphic tumors (adj. p 0.008, **Table 2**). Altered MYC status (by FISH or IHC) also tended to correlate with *TP53* mutations (adj. p 0.05 and 0.06, respectively), and 9 cases harboured both *TP53* mutations and *MYC* gene rearrangement (n=4) or copy gains (n=5) (**Figure 1, Supplemental Figure S3D-3F** and **Supplemental Table S4**).

Treatment and outcome

Treatments and outcomes of 63 patients are summarized in **Table 1**. Most patients (59/63, 93%) underwent surgery and tumor resection. Seventeen patients with no further treatment died within a median time of one month. Of 43 patients who received a first-line therapy, one died before assessment and 20 progressed on

treatment. Nine of 28 patients aged ≤65 years received consolidation with hematopoietic cell transplantation either autologous (auto-HCT) (n=8) or allogeneic (allo-HCT) (n=1). The 36 patients who relapsed following first-line therapy, often received one (or less commonly more) salvage treatment (30/36) and all died, usually from disease progression (n=31).

After a median follow-up of 46 months (alive patients), median overall survival (OS) was 7.8 months (rang 0-71). One-year and 2-years OS were 31% and 15%, respectively. In univariate analysis of OS (**Figure 5, Supplemental Table S6**): age>70, enterostomy, poor performance status (PS) (>2), advanced Lugano stage (≥2), lack of complete response to first-line therapy, atypical histology, MYC expression, and *TP53* mutations all were significantly associated with inferior outcome. Conversely, B-cell marker expression was associated with a better prognosis. The multivariate analysis confirmed the independent impact of *TP53* mutations (p=0.005, HR=5.83), *STAT5B* mutations (p=0.007, HR=3.67), B-cell (CD20 and/or CD79a) marker expression (p=0.005, HR=0.15) and poor PS (p=<0.001, HR=7.58) on OS (**Table 3, Supplemental Table S7**).

Eight patients survived beyond 24 months (**Supplemental table S8**). They all had a good PS at diagnosis and underwent surgery. The seven patients who received chemotherapy (CHOP-based in 5) reached complete (6) or partial (1) response. Six cases were classified as typical and two as atypical, all lacked *TP53* mutations, and MYC expression, and 4/8 were CD20+. In a very long survivor patient (#31) who relapsed five years after initial diagnosis, the relapsing tumor was also analyzed and showed a morphology and mutation profile identical to the initial diagnosis, and a very similar phenotype apart from reduced CD56 expression at relapse.

Discussion

This integrative clinical, histopathological and genetic analysis of 71 MEITL patients from Western Europe represents the largest study to date.

Our findings confirm that MEITL shows a rather homogeneous CD3+, CD4-, CD5-, CD7+, CD8+, CD56+ activated cytotoxic immunophenotype[4,5,10-14,17,18]. Most cases were CD8+ CD56+ and those negative for CD8 and/or CD56 (23%) did not show peculiar features. The distribution of TCR expression profiles is in line with the preferential γδ T-cell derivation reported in several studies[4,5,11,17]. In addition, TCRγδ+ and TCRαβ+ tumors showed similar pathological and mutational features, with no impact on outcome. Expression of CD103 (the α E subunit of the heterodimer integrin αEβ7), which is characteristic of intraepithelial lymphocytes of the small intestine and documented in T-cell lymphomas, particularly EATL[27], was positive in most cases, albeit with heterogeneous staining. CD103 expression could therefore represent an additional diagnostic feature of MEITL.

The mutational analyses reflect a very characteristic pattern of alterations involving frequent somatic deleterious alterations of *SETD2* (96%) and activation of JAK/STAT pathway gene(s), confirming our original discovery[7]. Moreover, *TP53* mutations and MYC deregulation occurred in a subset of cases. Intriguingly, while we also found 100% *SETD2* alterations in 9/9 cases from Japan[23], a lower incidence of *SETD2* mutations was reported in other series, being ~70% in 23 Northern American cases[6] and 22% in 20 Chinese cases[18]. Along with the notion of many tumor suppressor genes requiring biallelic inactivation[28], most cases had two *SETD2* alterations, with no evidences of germline variants. Notably, cases with apparently only one genetic hit had similarly reduced H3K36me3 histone mark, alluding to other mechanisms at play. Since functional studies have established the role of *SETD2*

ablation in driving experimental lymphomagenesis[29], our data support the key role of *SETD2* inactivation in MEITL pathogenesis. Conversely, mutations in other genes involved in DNA (and histone) methylation, in particular *TET2* and *DNMT3A*, were distinctly rare or absent contrasting with other T-cell lymphoma entities[30,31]. Thus, deregulated methylation of the H3K36 position represents the major epigenetic alteration in MEITL. For diagnostic purposes, NGS approaches interrogating the complete sequence of *SETD2* gene are mandatory since mutations are distributed without hot spots. In addition, we recommend analyses for the detection of *SETD2* locus loss or LOH. We showed that H3K36me3 immunohistochemistry is an acceptable surrogate or complement to genotyping.

We identified two groups of tumors with distinct morphological features: a typical group of monomorphic tumors (58%) and an atypical group of tumors (42%), non-monomorphic, or presenting features suggesting a more aggressive biology. Some nuclear pleomorphism and large cell morphology have been recognized in Asian series but no association to clinical features or divergent immunophenotypes has been reported[10,11,13,14,16,17]. Here, while both groups shared similar immunophenotype and heterogeneous T-cell lineage derivation, the atypical group had more frequent MYC expression, *TP53* alterations, and a shorter overall survival in univariate analysis. Thus, our novel findings confirm and expand the notion that MEITL comprises a morphological spectrum, irrespective of ethnicity, including an atypical subgroup with meaningful biological attributes, and clinical relevance. The recognition that MEITL may show pleomorphism, angiotropism, necrosis, high-grade features or inflammation, is important for pathologists and relevant to diagnosis. It implies to consider atypical MEITL in the differential diagnosis of aggressive pleomorphic intestinal T-cell tumors, including EATL, EBV-associated extranodal

NK/T-cell lymphoma, and intestinal T-cell lymphoma, NOS, which can be performed by the integration of clinical, immunophenotypic, H3K36me trimethylation status and mutational profile.

Median OS was only 7.8 months, on the lower end of the 7-15 months previously reported[9,10,18,24,32] perhaps related to the older age of our population and to a late diagnosis by an abdominal complication in most patients. Among baseline clinical parameters, univariate analysis found that age >70 years, PS >2 and Lugano stage ≥2 associated with a worse prognosis. However, in multivariate analysis only PS > 2 remained significantly associated with poor OS underlying the importance of patients' fitness to survive initial disease presentation and treatment. In addition, our study revealed biomarkers of independent unfavorable prognostic significance including *TP53* and *STAT5B* mutations and MYC expression. *TP53* alterations are well-known determinants of chemoresistance and worse outcome in lymphoma patients in general, and specifically in T-cell lymphomas[33-36]. Activating mutations of *STAT5B* mutations have an established role in T-cell lymphomagenesis[37]; they are frequent in several types of –usually aggressive- lymphomas derived from gamma-delta or NK cells, and in a subset of T-large granular lymphocytic leukemias (T-LGL)[21,22,29,38,39] associated with a more aggressive behaviour[38]. Accordingly, we found a striking negative effect of concurrent *TP53* and *STAT5B* mutations on survival.

In MEITL, gains of 8q24 or *MYC* copy gains have been variably reported in 25-70% of cases[5,10,11,40], rare cases harbouring *MYC* rearrangements have been described[10,19], and around half of cases reportedly show MYC protein expression[5,15,19]. We found MYC expression in one third of the cases, more frequently in atypical cases and in association with *TP53* mutations. Nine cases had

concurrent *MYC* and *TP53* gene alterations, with 6/7 patients dying within 5 months after diagnosis. The poor prognosis of patients with *MYC* plus *TP53* abnormalities has been reported in diffuse large B-cell lymphoma[41] along with high-grade morphology and also in chronic lymphocytic leukemia[42]. Thus, *MYC* and *TP53* aberrations may play a role in MEITL pathogenesis and progression.

In this study, chemoresistance to first-line CHOP-based polychemotherapy was high, even compared to other T-cell lymphomas[43], let alone that only 2/3 of patients had attempted systemic treatment after surgery. Yet, very few patients achieved CR during salvage and all eventually died of treatment toxicity or lymphoma progression. Certainly, there is an unmet medical need to improve treatment. Timely diagnosis and better supportive measures may help to reduce early mortality by improving the PS of MEITL patients and decrease toxicity of first-line therapy in a rapidly growing disease. CHOP-based polychemotherapy was mostly ineffective in our patients; therefore, alternative approaches are urgently needed. Remarkably, 5 of the 6 patients treated with the Ifosfamide, Etoposide, Epirubicin and Methotrexate (IVE-MTX) regimen followed by ASCT proposed for EATL reached CR, but only one survived > 24 months[44]. Of note, MEITL and hepatosplenic T-cell lymphoma (HSTL) are both aggressive extranodal chemoresistant diseases, which share biological characteristics[29,45]. Hence, non-CHOP first-line alternative polychemotherapy[46] such as ICE (ifosfamide, carboplatin, etoposide) or IVAC (ifosfamide, etoposide, high-dose cytarabine) followed by systematic consolidation, as recommended by the ESMO guidelines[47] could also be valuable for MEITL. Encouraging results have been reported after first-line auto-HCT[44,48] in both EATL and MEITL[24]. Herein patients receiving first-line HCT had longer OS, but HCT had been offered to young patients achieving CR, hence pre-selecting patients with a better prognosis. Consolidation

with allo-HCT has the best potential for relapse prevention in T-cell lymphoma but its use is limited by its toxicity[49]. In MEITL, allo-HCT could be recommended even first-line in eligible patients.

A better understanding of MEITL biology may open the path to innovative treatments beyond chemotherapy and transplantation. Particularly, the aberrant expression of B-cell markers, rare in T-cell lymphoma[50] raises the question of therapies targeting CD20 or CD79, while the lack of CD30 expression discourages the use of Brentuximab Vedotin. Given the frequent activation of the JAK-STAT pathway the use of JAK inhibitors may be useful[29]. The MEITL-hallmark loss of H3K36 trimethylation, confers high sensitivity to WEE1 kinase inhibitors[51], such as adavosertib, which is developed in clinical trials for solid tumors and could be evaluated in MEITL.

References

1. Jaffe ES, Chott A, Ott G, et al. Intestinal T-cell lymphoma. In Swerdlow SH, Campo E, Harris NL editors. WHO Classification of tumours of Haematopoietic and Lymphoid Tissues, revised 4th ed. Lyon, France: IARC Press; 2017. p372-80.
2. Vose J, Armitage J, Weisenburger D, International T-Cell Lymphoma Project. International peripheral T-cell and natural killer/T-cell lymphoma study: pathology findings and clinical outcomes. J Clin Oncol. 2008;26(25):4124-4130.
3. Laurent C, Baron M, Amara N, et al. Impact of Expert Pathologic Review of Lymphoma Diagnosis: Study of Patients From the French Lymphopath Network. J Clin Oncol. 2017;35(18):2008-2017.
4. Chott A, Haedicke W, Mosberger I, et al. Most CD56+ intestinal lymphomas are CD8+CD5-T-cell lymphomas of monomorphic small to medium size histology. Am J Pathol. 1998;153(5):1483-1490.
5. Takeshita M, Nakamura S, Kikuma K, et al. Pathological and immunohistological findings and genetic aberrations of intestinal enteropathy-associated T cell lymphoma in Japan. Histopathology. 2011;58(3):395-407.
6. Moffitt AB, Ondrejka SL, McKinney M, et al. Enteropathy-associated T cell lymphoma subtypes are characterized by loss of function of SETD2. J Exp Med. 2017;214(5):1371-1386.
7. Roberti A, Dobay MP, Bisig B, et al. Type II enteropathy-associated T-cell lymphoma features a unique genomic profile with highly recurrent SETD2 alterations. Nat Commun. 2016;7:12602.
8. Delabie J, Holte H, Vose JM, et al. Enteropathy-associated T-cell lymphoma: clinical and histological findings from the international peripheral T-cell lymphoma project. Blood. 2011;118(1):148-155.
9. Tse E, Gill H, Loong F, et al. Type II enteropathy-associated T-cell lymphoma: a multicenter analysis from the Asia Lymphoma Study Group. Am J Hematol. 2012;87(7):663-668.
10. Tan SY, Chuang SS, Tang T, et al. Type II EATL (epitheliotropic intestinal T-cell lymphoma): a neoplasm of intra-epithelial T-cells with predominant CD8αα phenotype. Leukemia. 2013;27(8):1688-1696.
11. Tomita S, Kikuti YY, Carreras J, et al. Genomic and immunohistochemical profiles of enteropathy-associated T-cell lymphoma in Japan. Mod Pathol. 2015;28(10):1286-1296.
12. Sun J, Lu Z, Yang D, Chen J. Primary intestinal T-cell and NK-cell lymphomas: a clinicopathological and molecular study from China focused on type II enteropathy-associated T-cell lymphoma and primary intestinal NK-cell lymphoma. Mod Pathol. 2011;24(7):983-992.
13. Ko YH, Karnan S, Kim KM, et al. Enteropathy-associated T-cell lymphoma--a clinicopathologic and array comparative genomic hybridization study. Hum Pathol. 2010;41(9):1231-1237.
14. Akiyama T, Okino T, Konishi H, et al. CD8+, CD56+ (natural killer-like) T-cell lymphoma involving the small intestine with no evidence of enteropathy: clinicopathology and molecular study of five Japanese patients. Pathol Int. 2008;58(10):626-634.
15. Kikuma K, Yamada K, Nakamura S, et al. Detailed clinicopathological characteristics and possible lymphomagenesis of type II intestinal enteropathy-associated T-cell lymphoma in Japan. Hum Pathol. 2014;45(6):1276-1284.

16. Tan SY, de Leval L. Monomorphic epitheliotropic intestinal T-cell lymphoma. In WHO Classification of Tumors Editorial Board. Digestive system tumours, revised 5th ed. Lyon, France: IARC Press; 2019. p390-2.
17. Chan JK, Chan AC, Cheuk W, et al. Type II enteropathy-associated T-cell lymphoma: a distinct aggressive lymphoma with frequent γδ T-cell receptor expression. Am J Surg Pathol. 2011;35(10):1557-1569.
18. Chen C, Gong Y, Yang Y, et al. Clinicopathological and molecular genomic features of monomorphic epitheliotropic intestinal T-cell lymphoma in the Chinese population: a study of 20 cases. Diagn Pathol. 2021;16(1):114.
19. Huang D, Lim JQ, Cheah DMZ, et al. Whole-genome sequencing reveals potent therapeutic strategy for monomorphic epitheliotropic intestinal T-cell lymphoma. Blood Adv. 2020;4(19):4769-4774.
20. Nairismägi ML, Tan J, Lim JQ, et al. JAK-STAT and G-protein-coupled receptor signaling pathways are frequently altered in epitheliotropic intestinal T-cell lymphoma. Leukemia. 2016;30(6):1311-1319.
21. Küçük C, Jiang B, Hu X, et al. Activating mutations of STAT5B and STAT3 in lymphomas derived from γδ-T or NK cells. Nat Commun. 2015;6:6025.
22. Nicolae A, Xi L, Pham TH, et al. Mutations in the JAK/STAT and RAS signaling pathways are common in intestinal T-cell lymphomas. Leukemia. 2016;30(11):2245-2247.
23. Tomita S, Kikuti YY, Carreras J, et al. Monomorphic Epitheliotropic Intestinal T-Cell Lymphoma in Asia Frequently Shows SETD2 Alterations. Cancers (Basel). 2020;12(12).
24. Yi JH, Lee GW, Do YR, et al. Multicenter retrospective analysis of the clinicopathologic features of monomorphic epitheliotropic intestinal T-cell lymphoma. Ann Hematol. 2019;98(11):2541-2550.
25. de Leval L, Parrens M, Le Bras F, et al. Angioimmunoblastic T-cell lymphoma is the most common T-cell lymphoma in two distinct French information data sets. Haematologica. 2015;100(9):e361-364.
26. Lemonnier F, Dupuis J, Sujobert P, et al. Treatment with 5-azacytidine induces a sustained response in patients with angioimmunoblastic T-cell lymphoma. Blood. 2018;132(21):2305-2309.
27. Morgan EA, Pihan GA, Said JW, et al. Profile of CD103 expression in T-cell neoplasms: immunoreactivity is not restricted to enteropathy-associated T-cell lymphoma. Am J Surg Pathol. 2014;38(11):1557-1570.
28. Paige AJ. Redefining tumour suppressor genes: exceptions to the two-hit hypothesis. Cell Mol Life Sci. 2003;60(10):2147-2163.
29. McKinney M, Moffitt AB, Gaulard P, et al. The Genetic Basis of Hepatosplenic T-cell Lymphoma. Cancer Discov. 2017;7(4):369-379.
30. Lemonnier F, Couronné L, Parrens M, et al. Recurrent TET2 mutations in peripheral T-cell lymphomas correlate with TFH-like features and adverse clinical parameters. Blood. 2012;120(7):1466-1469.
31. Couronné L, Bastard C, Bernard OA. TET2 and DNMT3A mutations in human T-cell lymphoma. N Engl J Med. 2012;366(1):95-96.
32. Haddad PA, Dadi N. Clinicopathologic Determinants of Survival in Monomorphic Epitheliotropic Intestinal T-Cell Lymphoma (MEITL): Analysis of a Pooled Database. Blood. 2020;136 (S1):28.
33. Young KH, Weisenburger DD, et al. Mutations in the DNA-binding codons of TP53, which are associated with decreased expression of TRAILreceptor-2, predict for poor survival in diffuse large B-cell lymphoma. Blood. 2007;110(13):4396-4405.

34. Chapuy B, Stewart C, Dunford AJ, et al. Molecular subtypes of diffuse large B cell lymphoma are associated with distinct pathogenic mechanisms and outcomes. Nat Med. 2018;24(5):679-690.
35. Kataoka K, Iwanaga M, Yasunaga JI, et al. Prognostic relevance of integrated genetic profiling in adult T-cell leukemia/lymphoma. Blood. 2018;131(2):215-225.
36. Watatani Y, Sato Y, Miyoshi H, et al. Molecular heterogeneity in peripheral T-cell lymphoma, not otherwise specified revealed by comprehensive genetic profiling. Leukemia. 2019;33(12):2867-2883.
37. Pham HTT, Maurer B, Prchal-Murphy M, et al. STAT5BN642H is a driver mutation for T cell neoplasia. J Clin Invest. 2018;128(1):387-401.
38. Rajala HL, Eldfors S, Kuusanmäki H, et al. Discovery of somatic STAT5b mutations in large granular lymphocytic leukemia. Blood. 2013;121(22):4541-4550.
39. López C, Bergmann AK, Paul U, et al. Genes encoding members of the JAK-STAT pathway or epigenetic regulators are recurrently mutated in T-cell prolymphocytic leukaemia. Br J Haematol. 2016;173(2):265-273.
40. Deleeuw RJ, Zettl A, Klinker E, et al. Whole-genome analysis and HLA genotyping of enteropathy-type T-cell lymphoma reveals 2 distinct lymphoma subtypes. Gastroenterology. 2007;132(5):1902-1911.
41. Deng M, Xu-Monette ZY, Pham LV, et al. Aggressive B-cell Lymphoma with MYC/TP53 Dual Alterations Displays Distinct Clinicopathobiological Features and Response to Novel Targeted Agents. Mol Cancer Res. 2021;19(2):249-260.
42. Chapiro E, Lesty C, Gabillaud C, et al. "Double-hit" chronic lymphocytic leukemia: An aggressive subgroup with 17p deletion and 8q24 gain. Am J Hematol. 2018;93(3):375-382.
43. Bachy E, Camus V, Thieblemont C, et al. Romidepsin Plus CHOP Versus CHOP in Patients With Previously Untreated Peripheral T-Cell Lymphoma: Results of the Ro-CHOP Phase III Study (Conducted by LYSA). J Clin Oncol. 2022;40(3):242-251.
44. Sieniawski M, Angamuthu N, Boyd K, et al. Evaluation of enteropathy-associated T-cell lymphoma comparing standard therapies with a novel regimen including autologous stem cell transplantation. Blood. 2010;115(18):3664-3670.
45. Travert M, Huang Y, de Leval L, et al. Molecular features of hepatosplenic T-cell lymphoma unravels potential novel therapeutic targets. Blood. 2012;119(24):5795-5806.
46. Voss MH, Lunning MA, Maragulia JC, et al. Intensive induction chemotherapy followed by early high-dose therapy and hematopoietic stem cell transplantation results in improved outcome for patients with hepatosplenic T-cell lymphoma: a single institution experience. Clin Lymphoma Myeloma Leuk. 2013;13(1):8-14.
47. d'Amore F, Gaulard P, Trümper L, et al. ESMO Guidelines Committee. Peripheral T-cell lymphomas: ESMO Clinical Practice Guidelines for diagnosis, treatment and follow-up. Ann Oncol. 2015;26 Suppl 5:v108-115.
48. Jantunen E, Boumendil A, Finel H, et al. Autologous stem cell transplantation for enteropathy-associated T-cell lymphoma: a retrospective study by the EBMT. Blood. 2013;121(13):2529-2532.
49. Schmitz N, Truemper L, Bouabdallah K, et al. A randomized phase 3 trial of autologous vs allogeneic transplantation as part of first-line therapy in poor-risk peripheral T-NHL. Blood. 2021;137(19):2646-2656.
50. Blakolmer K, Vesely M, Kummer JA, Jurecka W, Mannhalter C, Chott A. Immunoreactivity of B-cell markers (CD79a, L26) in rare cases of extranodal cytotoxic peripheral T- (NK/T-) cell lymphomas. Mod Pathol. 2000;13(7):766-772.

51. Pfister SX, Markkanen E, Jiang Y, et al. Inhibiting WEE1 Selectively Kills Histone H3K36me3-Deficient Cancers by dNTP Starvation. Cancer Cell. 2015;28(5):557-568.

Table 1: Clinical and biological features of MEITL at diagnosis.

Features	MEITL patients (n=71)
Median age, years (range)	67 (29-91)
Male, n (%)	36 (51%)
Medical History*	
Prior coeliac disease	0/62 (0%)
Previous cancer	6/62 (10%)
Auto-immune disease	2/62 (3%)
Symptom history median duration, months (range)**	<1m (0-20)
Abdominal pain	48/54 (89%)
Weight loss	34/54 (63%)
Fatigue	36/54 (67%)
Anorexia	28/54 (52%)
Diarrhea	15/54 (28%)
Palpable abdominal mass or adenopathy	10/54 (18%)
Acute event at presentation***	52/61 (85%)
Bowel perforation	43/61 (70%)
Bowel obstruction	17/61 (28%)
Performance Status	
0-1	27/56 (48%)
2	15/56 (27%)
>2	14/56 (25%)
Lugano stage	
Stage I	20/60 (33%)
Stage II	16/60 (27%)
II.1	9/60 (15%)
II.2	1/60 (2%)
IIE	3/60 (5%)
Not specified	3/60 (5%)
Stage IV	24/60 (40%)
Elevated serum LDH	18/32 (56%)
Hypoalbuminemia (<35g/L)	27/33 (82%)
Surgical management	59/63 (94%)
No chemotherapy	19/62 (31%)
First-line regimens	43/62 (69%)
CHOP-based (CHOP, CHOEP, Ro-CHOP, R-CHOP)	32/43 (74%)
CHOP + IVE-MTX	6/43 (14%)
Other treatments (COP, ACVBP, DDGP, radiotherapy)	4/43 (9%)
Unknown	1/43 (2%)
First-line consolidation****	9/43 (21%)
Response (at end of first line)	
Complete response	15/43 (35%)
Partial response	4/43 (9%)
Stable disease	2/43 (5%)
Primary progression	20/43 (46%)
Death with unknown status	1/43 (2%)
Unknown	1/43 (2%)

Progression/relapse after first-line	36/42 (86%)
Salvage treatment after progression/relapse	30/36 (83%)
Salvage treatment consolidation	3/30 (10%)
Number of lines of treated patients : median, n (range)	1 (1-5)

Abbreviations: PS, Performance Status; CHOP, Cyclophosphamide, Doxorubicin, Vincristine, Prednisone; CHOEP, Cyclophosphamide, Doxorubicin, Vincristine, Etoposide, Prednisone; Ro-, Romidepsin; R-, Rituximab; IVE-MTX, Ifosfamide, Epirubicin, Etoposide, Methotrexate; COP, Cyclophosphamide, Vincristine, Prednisone; ACVBP, Doxorubicin, Cyclophosphamide, Vindesine, Bleomycin, Prednisone; DDGP, cisplatin, dexamethasone, gemcitabine, and pegasparaginase ; auto-HCT, autologous Haematopoietic Cell Transplantation, allo-HCT allogeneic Haematopoietic Cell Transplantation ; OS, Overall Survival.

**Cancer cases: colorectal cancer (n=1), cutaneous T-cell lymphoma (n=1), essential thrombocytemia (n=1), prostatic cancer (n=1), breast cancer (n=2). Autoimmune disease: autoimmune thyroiditis (n=1), giant cell arteritis (n=1).*

*** Other symptoms not reported in the table included night sweats (n=5), pruritus (n=2), bleeding, pancreatitis, pleural effusion, pulmonary embolism, abdominal abscess, intestinal ulcers (n=1 for each).*

****patients with perforation occurring after the start of chemotherapy are not included.*

***** including autoHCT (n=8) and alloHCT (n=1).*

Table 2. Morphological, immunophenotypical and molecular characteristics of typical and atypical groups.

	All cases (N=71)	**Typical (N=41)**	**Atypical (N=30)**	***adj p.***
Morphology				
Non-monomophic	18/71 (25.3%)	0/41 (0%)	18/30 (60%)	**<0.0001 ***
Necrosis	9/71 (12.6%)	0/41 (0%)	9/30 (30%)	**<0.0001 ***
Starry-sky/apoptosis	7/71(9.8%)	0/41 (0%)	7/30 (23.3%)	**0.002 ***
Angiotropism	18/64 (28.1%)	0/37 (0%)	18/27 (66.6%)	**<0.0001 ***
Lack of epitheliotropism	6/54 (11.1%)	2/35 (5.7%)	4/19 (21.0%)	0.169
Immunological markers				
CD8	64/71 (90.1%)	37/41 (90.2%)	27/30 (90%)	1.000
CD56	61/71(85.9%)	33/41 (80.4%)	28/30 (93.3%)	0.174
CD3	70/71(98.5%)	40/41 (97.5%)	30/30 (100%)	1.000
CD2	32/66 (48.4%)	16/37 (43.2%)	16/29 (55.1%)	0.457
CD5	2/70 (2.8%)	2/40 (5%)	0/30 (0%)	0.503
CD7	63/65 (96.9%)	38/38 (100%)	25/27 (92.5%)	0.169
CD4	4/70 (5.7%)	2/41 (4.8%)	2/29 (6.8%)	1.000
CD103	52/65 (80%)	29/38 (76.3%)	23/27 (85.1%)	0.532
CD30	1/64 (1.5%)	0/37 (0%)	1/27 (3.7%)	0.422
TIA1	65/68 (95.5%)	38/41 (92.6%)	27/27 (100%)	0.271
Granzyme B	50/66 (75.7%)	27/38 (71.0%)	23/28 (82.1%)	0.388
Perforin	39/62 (62.9%)	23/36 (63.8%)	16/26 (61.5%)	1.000
CD20	12/67 (17.9%)	7/40 (17.5%)	5/27 (18.5%)	1.000
CD79a	4/51 (7.8%)	1/32(3.1%)	3/19 (15.7%)	0.140
Epigenetics				
SETD2 (score >8)	8/55 (14.5%)	5/33 (15.1%)	3/22 (13.6%)	1.00
H3K36me3 (score >8)	6/67 (8.9%)	4/38 (10.5%)	2/29 (6.8%)	0.69
TCR expression				
TCRβ	21/65 (32.3%)	11/36 (30.5%)	10/29 (34.4%)	0.794
TCRγ/δ	32/64 (50%)	17/36 (47.2%)	15/28 (53.5%)	0.801
TCRαβ-TCRγδ+	27/62 (43.5%)	14/34 (41.1%)	13/28 (46.4%)	0.955
TCRαβ+TCRγδ-	15/62 (24.1%)	8/34 (23.5%)	7/15 (46.6%)	
TCRαβ+TCRγδ+	5/62 (8.0%)	3/34 (8.8%)	2/28 (7.1%)	
TCRαβ-TCRγδ-	15/62 (24.1%)	9/34 (26.4%)	15/62 (24.1%)	
Cell cycle				
Ki-67 >50%	48/68 (70.5%)	24/39 (61.5%)	24/29 (82.7%)	0.066
MYC >25%	18/54 (33.3%)	5/30 (16.6%)	13/24 (54.1%)	**0.008**
p53 IHC mutated pattern	22/56 (39.2%)	6/31 (19.3%)	16/25 (64%)	**0.001**
Genetics				
TP53 mutation	22/64 (34.3%)	6/36 (16.6%)	16/28 (57.1%)	**0.001**
MYC alteration	12/60 (20%)	5/33 (15.1%)	7/27 (25.9%)	0.345
SETD2 alteration	62/64 (96.8%)	36/36 (100%)	26/28 (92.8%)	0.188

STAT5B mutation	37/65 (56.9%)	20/37 (54.0%)	17/28 (60.7%)	0.622
JAK3 mutation	32/64 (50%)	19/36 (52.7%)	13/28 (46.4%)	0.801

* Expected correlation (by definition)

Table 3. Multivariate model of overall survival.

N=44	**HR**	**95% CI**	***P value***
B-cell marker expression (IHC)	0.15	0.05 – 0.46	*0.001*
***TP53* mutation**	4.86	1.75 – 13.5	*0.002*
***STAT5B* mutation**	3.42	1.44 – 8.13	*0.005*
MYC expression > 25% (IHC)	3.06	1.33 – 7.04	*0.009*
Performance Status ≥2	6.46	2.44 – 17.1	*<0.001*

Abbreviation: IHC, immunohistochemistry; CI, confidence interval; HR: Hazard-Ratio

For multivariable analysis, the covariates were determined according to univariate results (P≤0.10) and to the clinical and biological relevance, restricted to 44 cases with available pretherapeutic features (**Supplemental Table S7, Supplemental Statistical methods**).

Figure legends

Figure 1. **Heatmap representation of morphological, immunophenotypical and molecular features of 71 monomorphic epitheliotropic intestinal T-cell lymphoma (MEITL) patients**.

Figure 2. **Typical MEITL cases #30 (A-C) and #51 (D-L). (A)** The intestinal tumor comprises a central transmural zone and a peripheral zone with intramucosal tumor spread. **(B)** The tumor cells are medium-sized and monomorphic with clear and ample cytoplasm and invade the epithelium of the crypts. **(C)** The tumor recurrence after five years shows an identical cytomorphology. **(D)** Intramucosal tumor spread is associated with shortening and widening of the villi. **(E)** Broadly expanded villi comprise a heavy epitheliotropic tumor cell infiltrate. **(F)** The tumor cells are strongly positive for CD3, **(G)** negative for CD5, **(H)** positive for CD8, **(I)** CD56, and **(J)** TCRβ. **(K)** CD103 is strongly positive in the superficial intramucosal tumor compartment and gradually decreases in the infiltrating part. **(L)** Lymphoma cells in the mucosa (upper part of panel figure) and submucosa (lower part of panel figure) are strongly and moderately positive for CD103. Original magnifications x10 (A), x40(K), x100 (E), x125 (D), x400 (B, C, F-J, L).

Figure 3. Atypical MEITL cases #31 (A-L), #15 (M) and #59 (N-P). (A) The tumor is composed of medium–sized pleomorphic cells and comprises scattered histiocytes with apoptotic debris. **(B)** A vein is infiltrated by lymphoma cells. **(C)** The lymphoma cells are weakly positive for TCRγ. **(D)** FISH with *SETD2* probe shows one red (*SETD2*) and two green (control) signals per nucleus, indicating deletion of one allele. **(E)** The lymphoma cells show strong nuclear positivity for H3K36me2 and **(F)** are

completely negative for H3K36me3, while reactive histiocytes are positive. **(G)** The lymphoma cells are diffusely positive for TIA-1, **(H)** show a high Ki67 index (>80%), and **(I)** are strongly positive for p53. **(J)** A gastric biopsy performed during follow-up showed recurrent tumor with a more blastoid morphology, invading the glandular epithelium. **(K)** Post-mortem liver showed lymphoma infiltrating in the sinusoids and within hepatocytes. **(L)** A cytokeratin immunostains confirmed emperipolesis of lymphoma cells into hepatocytes. **(M)** This case features marked angiotropism and angioinvasion. **(N)** This tumor contains large necrotic areas in its invasive portion, and **(O)** is composed of pleomorphic large cells. Original magnifications: x25 (N), x100(B, M), ×400 (A, C, E-K, L, O), X630(D).

Figure 4. Overview of the genetic alterations in MEITL. (A) Heatmap representation of mutations in a selected panel of genes examined by whole exome sequencing and targeted deep sequencing in 65 MIELT tumors. Patients are displayed as columns and mutations (named on the left) are coloured by the type of alteration. The percentage of mutated samples is represented on the right. First row shows the expression patterns of TCR isoforms, second row shows the status of H3K36me3 trimethylation and third row displays the results of *SETD2* FISH study. **(B)** Schematic representation of somatic mutations in *SETD2* (top), *STAT5B* (central) and *JAK3* (bottom) genes identified in this study. Domains of the protein are represented according to the Uniprot database (http://www.uniprot.org) in different colours. Exact positions of mutations found in MIETL cases are given, which are coloured by the type of alteration.

Figure 5. Overall survival for MEITL patients. (A) OS in months of the all cohort; and according to **(B)** age at diagnosis, **(C)** Performance Status score, **(D)** Lugano stage at diagnosis, **(E)** the presence of atypical histological features, **(F)** cytological

atypia, **(G)** *TP53* mutational status, **(H)** *STAT5B* mutational status, **(I)** the concurrent presence of *TP53* and *STAT5B* mutations and **(J)** MYC expression (>25% IHC). Abbreviations: # at risk, number at risk; OS, Overall Survival; PS, Performance Status; mut, mutated; WT, wild-type.

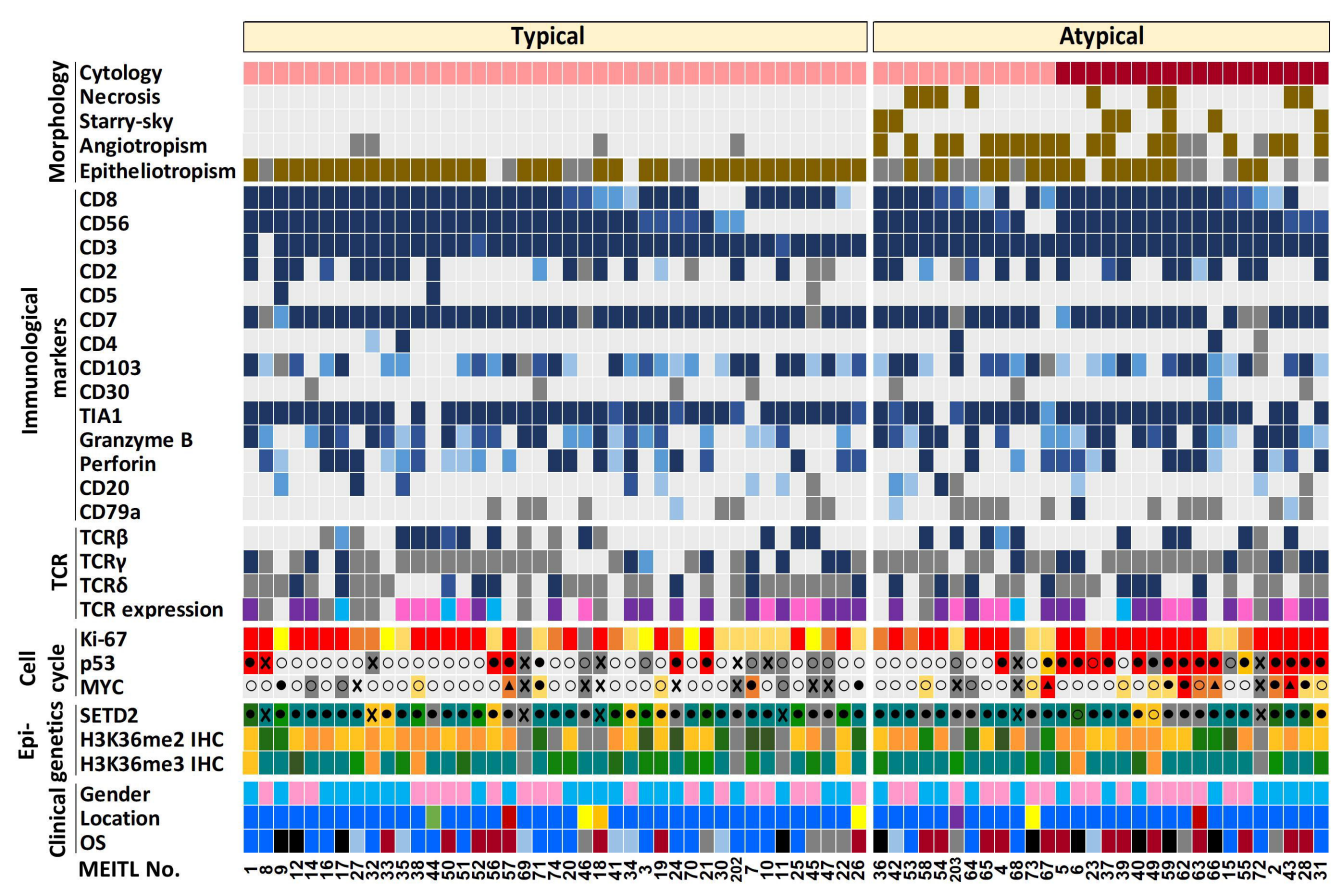

Morphology
- Monomorphic
- Non-monomorphic
- Features present
- Features absent
- No data

IHC
- <5%
- 5-25%
- 26-50%
- 51-75%
- 76-100%
- NA

TCR
- TCRαβ-TCRγδ+
- TCRαβ+TCRγδ-
- TCRαβ+TCRγδ+
- TCRαβ-TCRγδ-
- NA

Ki-67
- <25%
- 25-50%
- 51-75%
- 76-100%
- NA

p53
- >50%
- 0%
- ≤50%
- NA
- ● *TP53* mutated
- ○ *TP53* wild-type
- × No NGS data

MYC
- <25%
- 25-50%
- 51-75%
- 76-100%
- NA
- ● *MYC* copy gain
- ▲ *MYC* rearrangement
- ○ Normal FISH *MYC*
- × No FISH data

SETD2/H3K36
- Score 0
- Score 1
- Score 2
- Score 3
- Score 4
- Score 6
- Score 8
- Score 9
- Score 12

***SETD2* alterations**
- ● Present
- ○ Absent
- × No data

Gender
- Male
- Female

Location
- Small intestine
- Colon
- Stomac
- Anus
- Lymph node
- Epiplon

OS (months)
- < 1
- 1-5
- 6-24
- >24
- NA

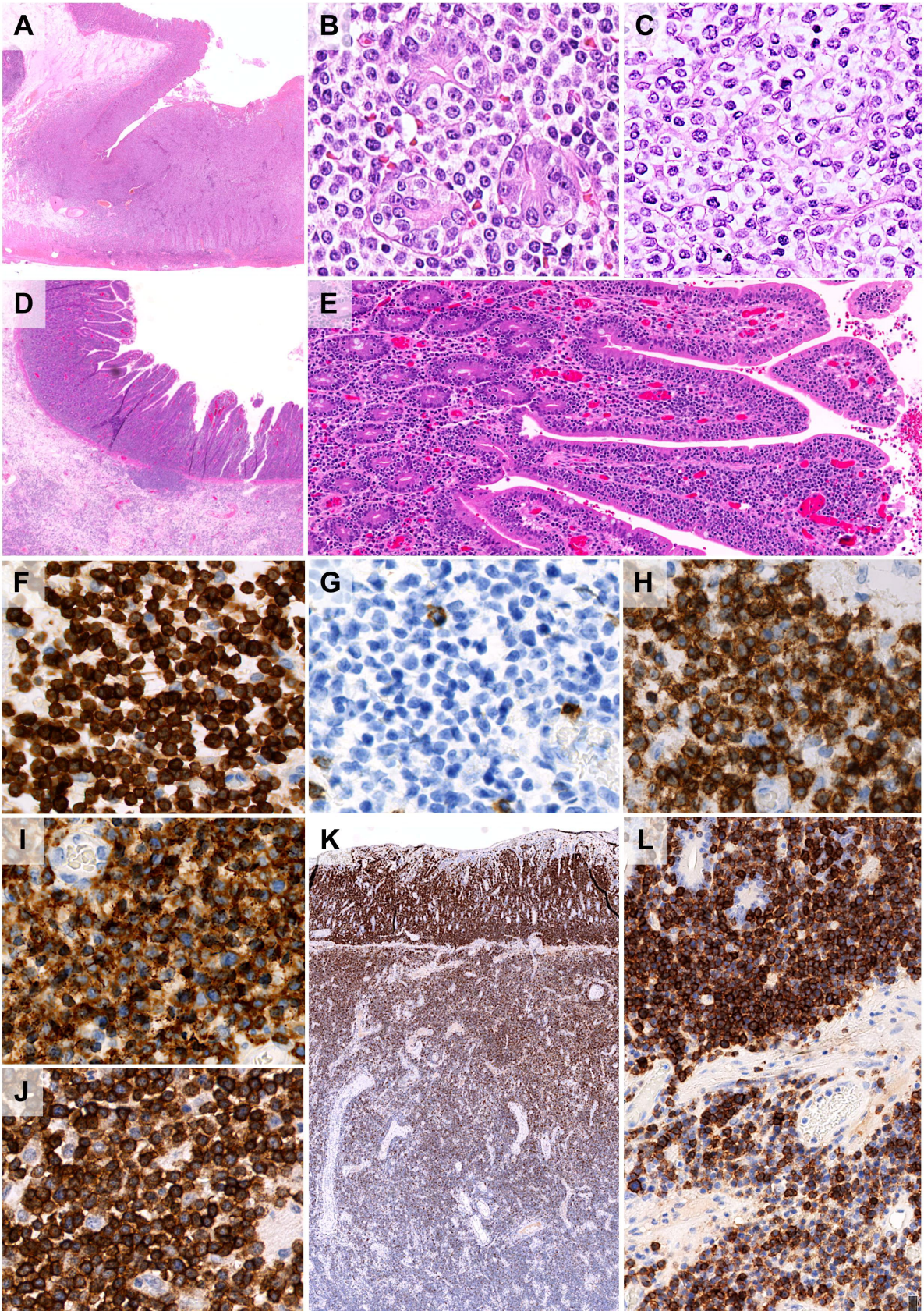
A
B
C
D
E
F
G
H
I
K
L
J

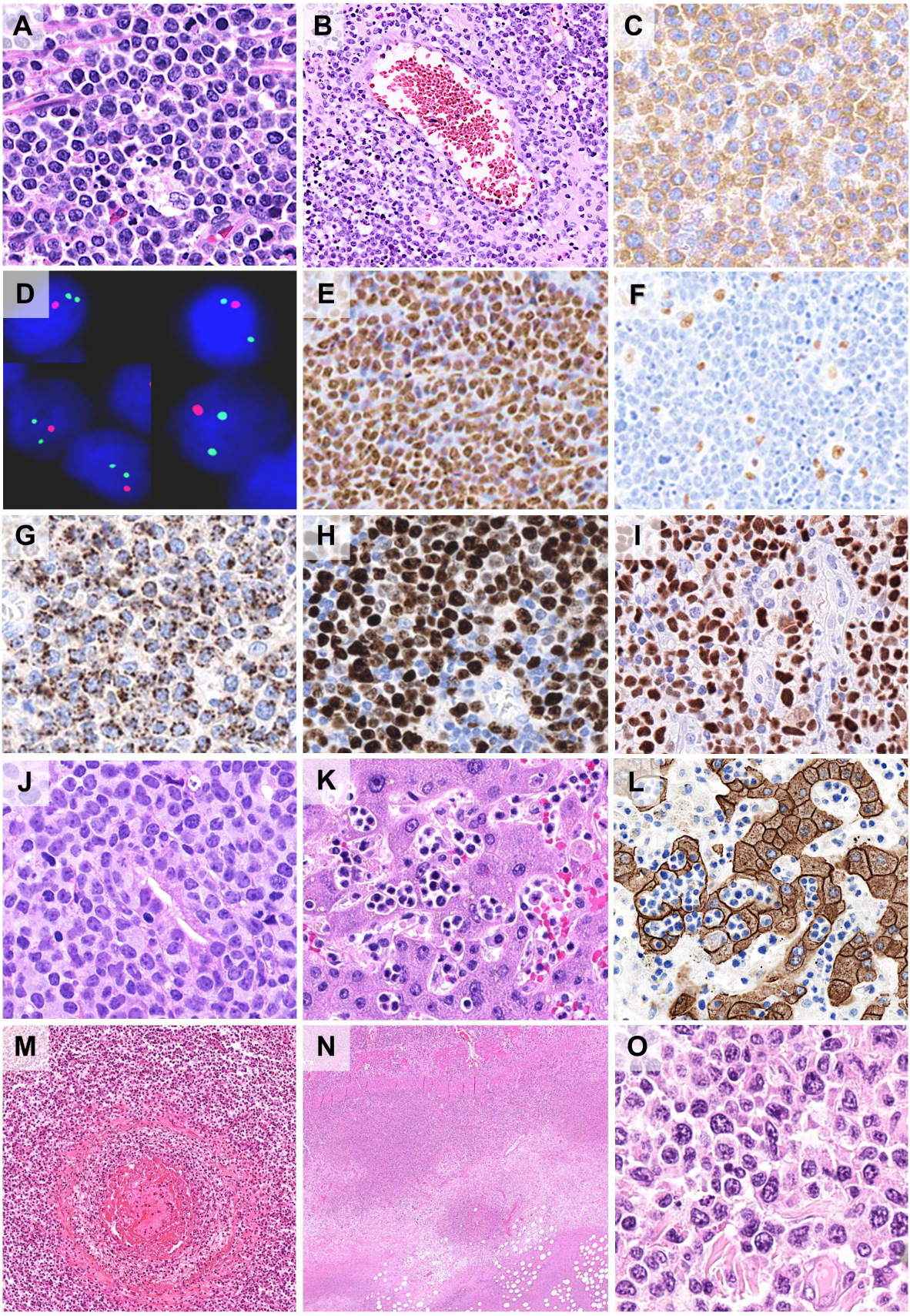
A
B
C
D
E
F
G
H
I
J
K
L
M
N
O

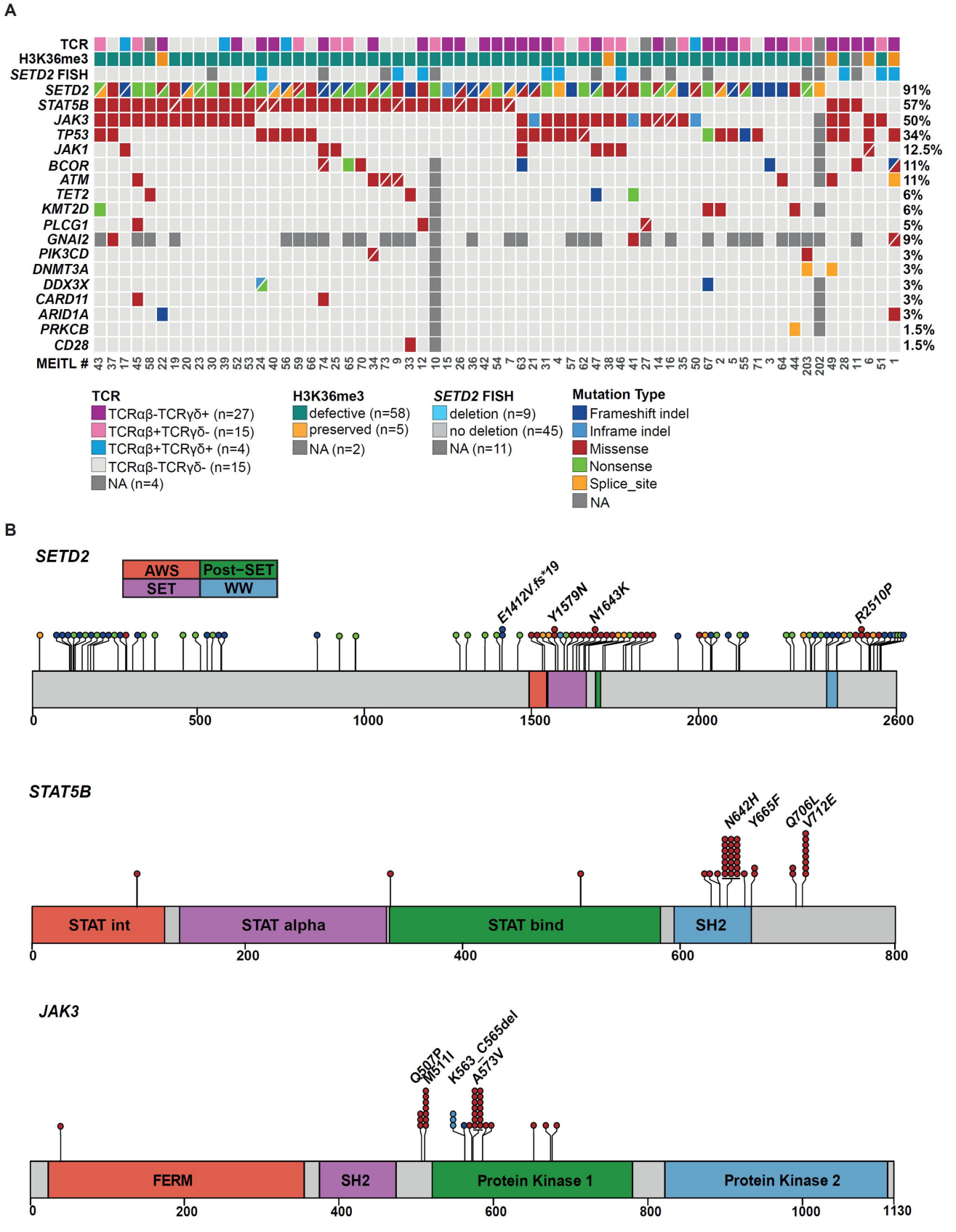
A
TCR
H3K36me3
SETD2 FISH
SETD2
STAT5B
JAK3
TP53
JAK1
BCOR
ATM
TET2
KMT2D
PLCG1
GNAI2
PIK3CD
DNMT3A
DDX3X
CARD11
ARID1A
PRKCB
CD28
MEITL #
91%
57%
50%
34%
12.5%
11%
11%
6%
6%
5%
9%
3%
3%
3%
3%
3%
1.5%
1.5%
TCR
TCRαβ-TCRγδ+ (n=27)
TCRαβ+TCRγδ- (n=15)
TCRαβ+TCRγδ+ (n=4)
TCRαβ-TCRγδ- (n=15)
NA (n=4)
H3K36me3
defective (n=58)
preserved (n=5)
NA (n=2)
SETD2 FISH
deletion (n=9)
no deletion (n=45)
NA (n=11)
Mutation Type
Frameshift indel
Inframe indel
Missense
Nonsense
Splice_site
NA
B
SETD2
AWS
Post−SET
SET
WW
E1412Vfs*19
Y1579N
N1643K
R2510P
0
500
1000
1500
2000
2600
STAT5B
N642H
Y665F
Q706L
V712E
STAT int
STAT alpha
STAT bind
SH2
0
200
400
600
800
JAK3
Q507P
M511I
K563_C565del
A573V
FERM
SH2
Protein Kinase 1
Protein Kinase 2
0
200
400
600
800
1000
1130

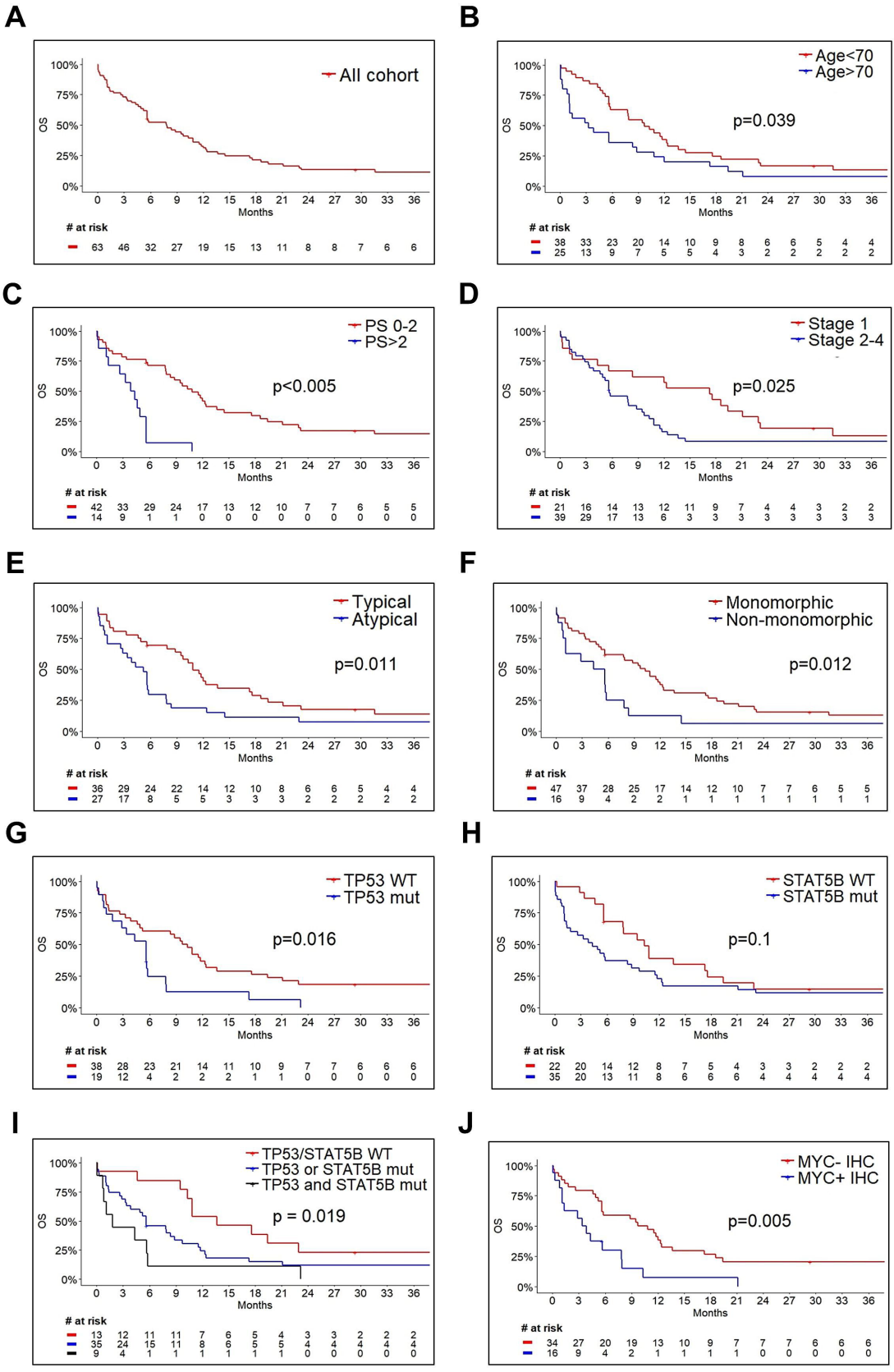
A
All cohort
OS
100%
75%
50%
25%
0%
0 3 6 9 12 15 18 21 24 27 30 33 36
Months
at risk
63 46 32 27 19 15 13 11 8 8 7 6 6
B
Age<70
Age>70
p=0.039
OS
Months
at risk
38 33 23 20 14 10 9 8 6 6 5 4 4
25 13 9 7 5 5 4 3 2 2 2 2 2
C
PS 0-2
PS>2
p<0.005
OS
Months
at risk
42 33 29 24 17 13 12 10 7 7 6 5 5
14 9 1 1 0 0 0 0 0 0 0 0 0
D
Stage 1
Stage 2-4
p=0.025
OS
Months
at risk
21 16 14 13 12 11 9 7 4 4 3 2 2
39 29 17 13 6 3 3 3 3 3 3 3 3
E
Typical
Atypical
p=0.011
OS
Months
at risk
36 29 24 22 14 12 10 8 6 6 5 4 4
27 17 8 5 5 3 3 3 2 2 2 2 2
F
Monomorphic
Non-monomorphic
p=0.012
OS
Months
at risk
47 37 28 25 17 14 12 10 7 7 6 5 5
16 9 4 2 2 1 1 1 1 1 1 1 1
G
TP53 WT
TP53 mut
p=0.016
OS
Months
at risk
38 28 23 21 14 11 10 9 7 7 6 6 6
19 12 4 2 2 2 1 1 0 0 0 0 0
H
STAT5B WT
STAT5B mut
p=0.1
OS
Months
at risk
22 20 14 12 8 7 5 4 3 3 2 2 2
35 20 13 11 8 6 6 6 4 4 4 4 4
I
TP53/STAT5B WT
TP53 or STAT5B mut
TP53 and STAT5B mut
p = 0.019
OS
Months
at risk
13 12 11 11 7 6 5 4 3 3 2 2 2
35 24 15 11 8 6 5 5 4 4 4 4 4
9 4 1 1 1 1 1 1 0 0 0 0 0
J
MYC- IHC
MYC+ IHC
p=0.005
OS
Months
at risk
34 27 20 19 13 10 9 7 7 7 6 6 6
16 9 4 2 1 1 1 1 0 0 0 0 0

Supplementary material

Veloza L, Cavalieri D et al.

Monomorphic epitheliotropic Intestinal T-cell lymphoma comprises morphologic and genomic heterogeneity impacting outcome

Supplementary methods p. 2-10

Supplementary Tables p. 11-25

Table S1- S8

Supplementary Figures p. 26-43

Figure S1 – S8

References p. 44

Supplementary methods

Histology, immunohistochemistry, and FISH

All cases were reviewed, and diagnoses confirmed by the senior pathologists (LdL or PG). The tissues analysed comprised 68 gastrointestinal tumors, one omental mass and two abdominal lymph nodes. The latter three patients had clinical evidence of gastrointestinal involvement. The samples mostly consisted of surgical resections (n=62), or endoscopic or surgical biopsies (n=9). Sixty-three gastrointestinal samples were from the small intestine (12: ileum, 13: jejunum, 5: duodenum, unspecified 33); 3 were from the colon, and one each anal and gastric.

Immunohistochemistry was performed on 4 µm FFPE sections using specific antibodies (**Supplementary Table S1**) on automated immunostainers (BenchMark XT and Ultra; Ventana Medical Systems, Tucson, AZ). For the subset of cases previously published SETD2, H3K36me3 and H3K36me2 immunostainings had been performed manually[1].

Immunostainings were evaluated by eye-balling by estimating of the extent (<5%, 5-25%, 26-50%, 51-75%, 76-100%) and intensity (weak, moderate, strong) of the staining. Negative staining with no internal positive controls were considered non-contributive. In general, a threshold of 5% positivity extent was considered for positive score. For Ki-67, MYC and p53, staining were scored by quartiles (<25%, 26-50%, 51-75%, 76-100%). MYC was considered overexpressed when ≥ 25% of cells showed nuclear expression with moderate/strong intensity while a tumor was defined as *"p53* mutation pattern" positive when ≥ 50% of cells showed strong expression or when a complete lack of staining was observed. A high proliferation was defined as a Ki-67 immunostaining ≥ 50%. For SETD2, H3K36me3 and H3K36me2, immunostainings were scored (0 to 12) by multiplying extent (<10%: 0, 10-25%:1, 26-50%:2, 51-75%:3, 76-100%:5) and intensity (weak:1, moderate:2,

strong:3) of the staining as previously published[1]. Defective trimethylation was defined by H3K36me3 /H3K36me2 scores ratio < 1 and/or an H3K36me3 or SETD2 scores ≤ 6. Annotations and scorings were validated independently by two observers; discordant results were resolved by consensus with senior pathologists.

Chromogenic in situ hybridization for the detection of Epstein-Barr virus (EBV) was performed with EBV–encoded RNA (EBER) probes (INFORM, EBER Probe; Ventana Medical Systems), according to the manufacturer's recommendations, with an automated slide stainer (BenchMark XT; Ventana Medical Systems).

FISH labelling was performed using the ZytoLight FISH-Tissue Implementation Kit (ZytoVision, Bremerhaven, Germany) according to the manufacturer's protocol, with a minor modification (digestion with pepsin was performed for 13 min at 37°C). Subsequent steps of FISH labelling were carried out as previously described[1]. Labelled slides were analysed with a Zeiss AxioImager Z2 fluorescence microscope (Carl Zeiss, Oberkochen, Germany) equipped with specific filters for FITC, SpectrumOrange, DAPI, and double and triple band-pass filters. Hybridization signals were examined with a Plan-APOCHROMAT 63x oil immersion objective (Carl Zeiss). Images were captured using ISIS digital image analysis system version 5.5 (Metasystems, Altlussheim, Germany).

For evaluation of the *SETD2* locus, as previously described[1], we used a bacterial artificial chromosome (BAC) probe overlapping with the 3' end of the *SETD2* locus (target probe at 3p21.31: RP11-425J9, GenBank reference AC094020.2) labelled with orange, and two BAC clones hybridizing to the 3p25 region (control probe at 3p25: RP11-266J6 and RP11-485N3, GenBank references AC011610.11/AC022382.4 and AQ633871.1/AQ633873.1, respectively), labelled with green. At least 50 tumor nuclei were analysed for each case, and > 11.2% of nuclei with a ratio of orange to green signals ≤ 0.5 was considered indicative of *SETD2* deletion.

To detect *MYC* alterations, a commercial LSI *MYC* Dual Color Break Apart Rearrangement Probe (8q24) was used (Abbott Molecular, Des Plaines, IL, USA), and at least 50 nuclei were evaluated for each case. Cases were classified into *MYC* copy gain-positive if the average number of *MYC* copies per nucleus was ≥ 3. In case of *MYC* copy gain, the 3p25 control probe (used for *SETD2* locus evaluation, see above) was used to exclude a possible hyperploidy; the latter was considered in case of a concomitant *MYC* and 3p25 copy gain (average copies ≥ 3). *MYC* rearrangement was defined by > 10% of nuclei with split signals.

DNA isolation

Genomic DNA (gDNA) was extracted from unstained FFPE sections. Areas with highest tumor cell content and those devoid of neoplastic cells were marked on HE slides by a pathologist and subsequently reported on corresponding FFPE sections stained with toluidine blue. Manual microdissection of the regions of interest was performed under a microscope, followed by genomic DNA extraction using Maxwell® 16 Plus LEV DNA FFPE Purification Kit (Promega), according to the manufacturer's instructions. gDNAs were quantified by Qubit fluorometer (Thermo Fisher Scientific), and their quality and size distribution were assessed by capillary electrophoresis using Fragment Analyzer with High Sensitivity Genomic DNA Analysis Kit, following manufacturer's instructions.

Whole exome sequencing (WES)

Thirty-four cases were analyzed by WES, including, 14 previously reported[1]. For the remaining 20 samples, 500 ng of paired tumoral and normal DNA were sheared with Covaris S220 using AFA 520045 tubes and the following settings: duty Factor 10%; Peak Incident Power 175; Cycle/Busrt 200 and time 3 or 5 minutes depending on DNA quality. Libraries were performed using the Kapa Hyperplus library preparation kit (Roche,

Pleasanton, CA) combined to the xgen research panel v1.0 and UMIs (in order to identify PCR duplicates) from IDT DNA (Newark, New Jersey, USA). Captures were pooled further and paired-end sequenced on a HiSeq 4000 from Illumina (San Diego, CA). On average, around 80 million pair-end reads per sample were sequenced reaching a mean coverage of 204X (range 132-381) for tumor and 200X (range 115-380) for normals.

Targeted deep sequencing (TDS)

34 samples were subject to TDS using a customized panel covering 27 genes relevant to T-cell lymphoma biology (*ARID1A, ATM, BCOR, CARD11, CCR4, CD28, CTNNB1, DDX3X, DNMT3A, FYN, IDH2, IRF4, JAK1, JAK3, KMT2D, PIK3CD, PLCG1, PRKCB, RHOA, SETD2, SOCS1, STAT3, STAT5B, TET2, TNFRSF1B, TP53, VAV1*). Briefly, 100 to 200 ng of gDNA template was used to prepare DNA libraries with the KAPA HyperPlus library preparation kit (Roche, Pleasanton, CA). Target enrichment of the DNA libraries was performed by hybridization capture with a custom design of xGen Lockdown Probes (Integrated DNA Technologies, Coralville, IA) covering the full coding sequences of the targeted genes. Enriched libraries were sequenced on a MiSeq™ equipment (Illumina) as previously described[2]. On average, we sequenced around 2.5 million pair-end reads per sample reaching a mean coverage of 1858X (range 129-3491).

Sequence analysis

Sequence analysis was based on established algorithms and pipelines according to GATK best practices (The Genome Analysis Toolkit) standards (Best practice variant detection with the GATK v.4.1, for release 2.0). Initial QC steps involved demultiplexing, quality assessment of the produced reads and adapter removal. Forward and reverse reads were aligned to the human genome (GATK repository, build 37 decoy) using BWA-MEM (v0.7.10) [2]. BAM files were subjected to PCR duplicate removal using Unique Molecular

Indexes (fgbio v0.6.1) (WES analysis) or MarkDuplicates (Picard – for TDS analysis), followed by realignment around indels (GATK tools v3.7) and base recalibration using (GATK tools v4.1).

For WES analysis, the variant call was restricted to the 27 genes included in the TDS panel plus the *GNAI2* gene. Single nucleotide and indel variant calling was performed using VarScan (v2.4.4) and MuTect2 algorithm (GATK v4.1) comparing tumor *versus* matched normal. Specifically for VarScan, reads from normal and tumor samples were pileup using samtools mpileup (v1.9) with the following parameters: -x (disable read-pair overlap detection), -B (disable per-base alignment quality), -d 1000000 (max depth), -q 1 (skip alignment with mapQ smaller than 1), -C 50 (adjust mapping quality), -m 3 (min number gapped reads for indels candidates) and -F 0.0002 (min fraction of gapped reads). The tumor and normal pileup files were compared by VarScan somatic algorithm using the following parameters: minimum variant allele frequency threshold=0.01, tumor purity (tumor dependent), normal purity=0.95, minimum read depth at a position to make a call=10 and Somatic p-value=0.1 (Fisher's Exact Test). Variants were further filtered employing bam-readcount (-q 1, -b 20) and fpfilter algorithm in VarScan.

For MuTect, a set of 46 normal samples was used to generate a Pool of Normal (PON), which was applied into the tumor/normal comparison. Call was performed using defaults parameters, but keeping the option “genotype-pon-site” as true.

Variants were further filtered using the FilterMutectCalls algorithm as described in https://github.com/broadinstitute/gatk/blob/master/docs/mutect/mutect.pdf.

Calls from the two callers were combined in R, considering the union of the VarScan and MuTect callers.

Further variant filtering was carried out using the following formula: VAF Norm<15% & VAF Tum>=40% & Cov.REF Norm >=18 reads & Cov.ALT Tum>5 reads & (VAF Tum- VAF Norm)>=30% OR VAF Norm<10% & VAF Tum<=40% & VAF Tum>5% & Cov.REF Norm >=18 reads & Cov.ALT Tum>5 reads & (VAF Tum- VAF Norm)>=5%, where VAF Norm and VAF Tum represent the allele frequencies observed for the variant in normal and tumor, respectively; Cov.REF and Cov.ALT represent the local coverage observed for the reference or the alternative sequence, respectively. Variants with a “PASS” in the caller filter were also retained, while they were excluded if part of the false positive genes reported by Fajardo et al.[3] or if described to be a polymorphism with MAF (minimum allele frequency) of 1% in the 1000Genome project (v.Oct2014), NIH-Exome Sequencing Project (ESP6500 - European ancestry subset) or ExAC (r.1).

For TDS analysis, single nucleotide and indel variant calling was performed using VarScan (v2.4.3) and MuTect2 algorithm (GATK v3.7). Specifically for VarScan, reads from tumor sample were pileup using samtools mpileup (v1.3) with the following parameters: -x (disable read-pair overlap detection), -B (disable per-base alignment quality), -d 1000000 (max depth), -q 1 (skip alignment with mapQ smaller than 1), -C 50 (adjust mapping quality), -m 3 (min number gapped reads for indels candidates) and -F 0.0002 (min fraction of gapped reads). The tumor pileup file was further analyzed with VarScan mpileup2snp and mpileup2indel functions using the following parameters: minimum variant allele frequency threshold=0.01, minimum average quality 20, minimum coverage of 50 reads, minimum read depth at a position to make a call=10 and Somatic p-value=0.1 (Fisher's Exact Test).

For MuTect, call was performed using defaults parameters. The union of the variants called by VarScan and MuTect were combined in R and filter using the following parameters: local coverage above 50 reads, at least 10 reads supporting the variant and allele

frequency above 1%. Variants were further filter using an internal list of artefacts developed during the development and validation of the TDS panel. Furthermore, considering the potential presence of germinal variants, mutations were also filtered if present in the gnomAD database with more than 9 alleles in any populations (excluding Ashkenazi), when tumor allele frequency was above 40%.

All variants were finally annotated for presence in dbSNP, the ExAC (r.1) and COSMIC (v88) databases as well as mutation effect on gene transcript by SnpEff (v.4.3t). Only nonsynonymous variants or alterations occurring in the splice-sites (last 2 nucleotides of the exon and the first 10 nucleotides of the introns) were retain in the final table.

All retained alterations were confirmed by visual inspection with the Integrative Genomics Viewer (IGV) tool.

It should be noted that 24 samples were analyzed with both WES and TDS panel, showing complete agreement between the two analyses.

Statistical methods (extended)

The χ^2 test or Fisher's exact tests were used to determine associations between morphological, immunophenotypical and genetic characteristics of MEITL tumors. Estimates of overall survival were constructed using the Kaplan-Meier method. Cox proportional hazards regression model was used to investigate associated prognostic factors in univariate and multivariable analysis. The proportional-hazard hypothesis was verified using Schoenfeld's test and plotting residuals.

For multivariable analysis, the covariates were determined according to univariate results ($P \leq 0.10$) and to the clinical and biological relevance, restricted to available pretherapeutic features. A particular attention was paid on the multicolinearity and on the rules-of-thumb suggested for determining the minimum number of subjects required to conduct multiple

regression. Recommendations for sample size are heterogeneous and often with minimal empirical evidence. This is problematic because statistical procedures that create optimized combinations of variables tend to overfit the data. Thus, this overfitting can result in erroneous conclusions if models fit to one data set are applied to others.

Accordingly, the final multivariable model was built step by step, first focusing only on biological parameters (i) studying the relationships between the following covariables and (ii) evaluating the impact to add or delete them on multivariable analyses: B-cell marker expression, *TP53* mutation, *STAT5B* mutation, MYC expression (> 25%) and atypical histology). Following this step, atypical histology was excluded from multivariable analyses according to the significant relationship with *TP53* mutation, MYC expression.

The testing and parameter estimation performed using a statistical model clearly depends on the variables included in the model, it is therefore crucial for confounding adjustment that known clinically significant variables are included in the regression model. A clinically significant variable may well be an important confounder also when it is statistically insignificant. Then, clinical variables were included in multivariable analyses in addition to biological variables: performance status ≥2, age ≥70 and Lugano stage ≥2. Age and Lugano were not statistically significant. In final model, only performance status was retained with biological parameters.

The Akaike information criterion and Bayesian information criterion were calculated and used as model diagnostics to determine how well the model fit improved following addition of covariates. Results were expressed as hazard-ratio (HR) and 95% confidence interval.

Furthermore, to ensure the robustness of our results, the final model was validated by a two-step bootstrapping process. In each step, 1,000 bootstrap samples with replacements were created from the training set. In the first one, using the stepwise procedure, we determined the percentage of models including each of the initial variables. In the second step, we independently estimated the Cox model parameters of the final model. The

bootstrap estimates of each covariate coefficient and standard errors were averaged from those replicates.

A sensitivity analysis, including also age ≥70 and Lugano stage ≥2 in addition to aforementioned covariables (performance status and biological variables), was conducted. Statistical analysis was performed using Stata software (version 15, StataCorp LP, College Station, US). The tests were two-sided, with a type I error set at 5%. When appropriate, a correction of the type I error was applied to take into account multiple comparisons: Bonferroni method for the relationships between morphological, immunophenotypical and genetic characteristics of MEITL tumors and Sidak method for two by two multiple comparisons concerning overall survival.

Supplementary tables

Supplementary Table S1. List of antibodies used for immunohistochemical studies

Antibody	Clone	Source	Dilution
CD3	2GV6	Ventana Medical Systems, Tucson, AZ	RTU
CD20	L26	Novocastra, Newcastle, UK	1/400
CD2	AB75	Novocastra, Newcastle, UK	1/30
CD4	SP35	Ventana Medical Systems, Tucson, AZ	RTU
CD5	SP19	Abcam, Cambridge, UK	1/40
CD7	CBC.37	DakoCytomation; Agilent Technologies, Santa Clara, CA	1/25
CD8	C8/144B	DakoCytomation; Agilent Technologies, Santa Clara, CA	1/30
CD30	Ber-H2	DakoCytomation; Agilent Technologies, Santa Clara, CA	1/30
CD56	CD564	Novocastra, Newcastle, UK	1/25
CD79a	JCB117	DakoCytomation; Agilent Technologies, Santa Clara, CA	1/50
CD103	EPR4166	GeneTex, Irvine, CA	1/300
TIA-1	2G9A10F5	Beckman Coulter, Brea, CA	1/1000
Granzyme B	GrB-7	Monosan, Uden, The Netherlands	1/30
Perforin	5B10	Diagnostic Biosystem, Pleasanton, CA	1/10
PD1	NAT105	Ventana Medical Systems, Tucson, AZ	RTU
Ki-67	MIB-1	DakoCytomation, Agilent Technologies, Santa Clara, CA	1/50
TCRb-F1	8A3	Thermo Fisher Scientific, Waltham, MA	1/30
TCRγ	3.20	Thermo Fisher Scientific, Waltham, MA	1/100
TCRδ	H41	Santa Cruz, Dallas, TX	1/200
SETD2	Polyclonal	Sigma, Sigma-Aldrich, St. Louis, MO	1/200
H3K36me3	Polyclonal	Abcam, Cambridge, UK	1/200
H3K36me2	Polyclonal	Abcam, Cambridge, UK	1/250
PAX5	SP34	Ventana Medical Systems, Tucson, AZ	RTU
MYC	Y69	Ventana Medical Systems, Tucson, AZ	RTU
P53	DO-7	DakoCytomation, Agilent Technologies, Santa Clara, CA	1/500

Abbreviation: RTU, ready-to-use

Supplementary Table S2. Localizations and extension of MEITL tumors

GI tract involvement	100%	63/63
Small bowel only	73.0%	46/63
Small bowel + large bowel	17.5%	11/63
Small bowel + stomach	1.6%	1/63
Small bowel + no extension data*	4.8%	3/63
Large bowel only	1.6%	1/63
Anus only	1.7%	1/63
Small bowel involvement		
Duodenum only	6.6%	4/61
Jejunum only	23.0%	14/61
Ileum only	24.6%	15/61
Multi-site involvement	6.6%	4/61
Not specified	39.3%	24/61
Lymph node involvement**		
Infradiaphragmatic	48.3%	29/60
Supradiaphragmatic	16.7%	10/60
Both	10%	6/60
Extranodal/extraGI involvement**	31.7%	19/60
Lung	8.3%	5/60
Liver	6.7%	4/60
Pleura	5%	3/60
Bone marrow***	7.4%	2/27
Abdominal wall	3.3%	2/60
Pelvis	3.3%	2/60
Bladder	3.3%	2/60
Other sites****	8.3%	5/60

*In 3 patients a small bowel involvement was documented, but not data available for other gastrointestinal sites (CT/PET/surgery report). **In 3 patients, no extension data were available regarding lymph node extension and extranodal involvement. ***Only 27 patients had a bone marrow biopsy at diagnosis. **** Other sites included pancreas (n=1), kidney (n=1), spleen (n=1), testis (n=1), and sphenoïd sinus (n=1).

Supplementary Table S3. Biological findings in MEITL patients at diagnosis

Protein C reactive		
Normal	12.1%	5/41
05-50	24.4%	10/41
>50	63.4%	26/41
Kidney failure	17%	8/47
Elevated liver enzymes	9.5%	4/42
Hypercalcemia	2.5%	1/40
CSF involvement	0%	0/13
Positive coeliac serology*	0%	0/18

Abbreviation: CSF, cerebrospinal fluid involvement.

*Coeliac serology included screening for anti-endomysium, anti-transglutaminase and/or anti-gliadin antibodies.

Supplementary Table S4. Correlations between morphological, immunophenotypical and genetic characteristics of MEITL tumors

	Necrosis	Angiotropism/ angioinvasion	Starry-sky/apoptosis	Non-monomorphic	Atypical histology	Epitheliotropism	CD56+	CD8+	B-cell antigen expression	Activated cytotoxic+	CD103+	TCRγδ+TCRβ- (vs TCRγδ-TCRβ+)	KI-67 >50%	p53 mutated pattern IHC	*TP53* mutation	MYC IHQ >25%	*MYC* gene alteration	*STAT5B* mutation
Angiotropism/angioinvasion	0.09																	
Starry-sky/apoptosis	1	0.38																
Non-monomorphic	0.26	0.04	0.08															
Atypical histology	0.004	<0.001	0.02	<0.001														
Epitheliotropism	0.48	0.95	0.78	0.18	0.56													
CD56+	0.76	0.97	0.93	0.32	0.56	0.93												
CD8+	1	1	0.92	1	1	0.90	1											
B-cell antigen expression	0.76	1	1	1	1	1	1	0.76										
Activated cytotoxic +	0.94	0.95	1	1	0.97	0.93	1	0.65	0.58									
CD103+	0.95	1	0.76	1	0.92	1	0.76	1	0.97	0.95								
TCRγδ+TCRβ- (vs TCRγδ-TCRβ+)	1	0.97	1	0.97	1	0.92	1	0.73	0.97	0.26	1							
Ki-67 >50%	0.30	0.93	0.95	0.33	0.33	0.78	0.05	0.76	0.92	0.68	0.18	1						
P53 mutated pattern IHC	0.97	0.18	0.82	<0.001	0.01	0.11	0.95	0.95	0.92	0.48	1	1	0.61					
***TP53* mutation**	0.90	0.33	0.63	<0.001	0.02	0.35	0.52	0.76	0.92	0.66	1	0.92	0.56	<0.001				
MYC IHQ >25%	0.41	0.56	0.61	0.03	0.07	0.76	0.78	0.94	1	0.95	0.97	1	1	0.33	0.06			
***MYC* gene alteration**	0.78	0.90	0.95	0.35	0.76	0.35	0.59	0.70	0.78	0.76	0.95	1	0.35	0.13	0.05	<0.001		
***STAT5B* mutation**	0.33	1	0.48	1	0.95	0.78	0.56	1	0.48	0.97	0.06	0.92	0.73	0.56	0.33	1	1	
***JAK3* mutation**	0.90	0.93	1	0.93	1	0.95	0.76	0.76	1	0.90	0.59	0.76	0.01	1	1	0.93	0.76	0.48

Abbreviation: IHC, immunohistochemistry.

Red cell: positive correlation; blue cell: expected correlation (by definition)

The χ^2 test and Fisher's exact tests were used to determine associations between variables and groups. Two-sided $p<0.05$ were considered to be statistically significant. p-values were adjusted for multiple testing with Benjamini & Hochberg method.

Supplementary Table S5. List of mutations identified in MEITL patients by WES and targeted sequencing.

SampleID	Chrom.	Position	Ref	Alt	ExonicFunc.refGene	Cytoband	Gene Symbol	Reference ID	Results (HGVS.c, HGVS.p)	Allele Frequenc	Coverage	TDS‡	WES‡
MEITL-1	1	27101348	T	C	missense_variant	1p36	ARID1A	NM_006015.4	c.4630T>C (p.Ser1544Pro)	39.2%	199X	Nat Comm	Exome.Ag
MEITL-1	11	108121804	G	A	splice_donor_variant&splice_region_variant&intron_variant	11q22	ATM	NM_000051.3	c.1607+5G>A	40.23%	87X	Nat Comm	Exome.Ag
MEITL-1	17	7577532	G	A	missense_variant	17p13	TP53	NM_000546.5	c.749C>T (p.Pro250Leu)	44.44%	72X	Nat Comm	Exome.Ag
MEITL-1	3	50293695	G	A	missense_variant	3p21	GNAI2	NM_002070.3	c.536G>A (p.Arg179His)	34.92%	63X	Nat Comm	Exome.Ag
MEITL-1	3	50294174	C	A	missense_variant	3p21	GNAI2	NM_002070.3	c.613C>A (p.Gln205Lys)	35.48%	31X	Nat Comm	Exome.Ag
MEITL-1	X	39932851	GT	G	frameshift_variant	Xp11	BCOR	NM_001123383.1	c.1747del (p.Thr583Profs*6)	73.02%	63X	Nat Comm	Exome.Ag
MEITL-1	X	39933289	G	A	missense_variant	Xp11	BCOR	NM_001123383.1	c.1310C>T (p.Thr437Ile)	38.1%	168X	Nat Comm	Exome.Ag
MEITL-10	17	40359729	T	G	nonsynonymous SNV	17q21.2	STAT5B	NM_012448.3	c.1924A>C (p.Asn642His)	31.78%	815X	Nat Comm	none
MEITL-10	3	47162927	G	A	stopgain	3p21.31	SETD2	NM_014159.6	c.3199C>T (p.Gln1067*)	18.18%	1287X	Nat Comm	none
MEITL-11	17	40359659	T	A	missense_variant	17q21	STAT5B	NM_012448.3	c.1994A>T (p.Tyr665Phe)	42%	134X	NGSIyT	none
MEITL-11	X	39922118	C	T	missense_variant	Xp11	BCOR	NM_001123383.1	c.3952G>A (p.Asp1318Asn)	100%	86X	NGSIyT	none
MEITL-12	17	40354460	A	T	missense_variant	17q21	STAT5B	NM_012448.3	c.2135T>A (p.Val712Glu)	78.57%	14X	Nat Comm	Exome.Ag
MEITL-12	20	39794862	A	G	missense_variant	20q12	PLCG1	NM_002660.2	c.1828A>G (p.Ile610Val)	10.14%	217X	Nat Comm	Exome.Ag
MEITL-12	3	47143034	G	C	missense_variant	3p21	SETD2	NM_014159.6	c.4929C>G (p.Asn1643Lys)	82.76%	147X	Nat Comm	Exome.Ag
MEITL-14	19	17945912	G	C	missense_variant	19p13	JAK3	NM_000215.3	c.2027C>G (p.Pro676Arg)	54.94%	166X	Nat Comm	Exome.Ag
MEITL-14	19	17949108	C	T	missense_variant	19p13	JAK3	NM_000215.3	c.1533G>A (p.Met511Ile)	63.91%	135X	Nat Comm	Exome.Ag
MEITL-14	3	47147505	C	T	missense_variant	3p21	SETD2	NM_014159.6	c.4821G>A (p.Met1607Ile)	35.78%	563X	Nat Comm	Exome.Ag
MEITL-14	3	47161751	G	A	stop_gained	3p21	SETD2	NM_014159.6	c.4375C>T (p.Arg1459*)	47.18%	251X	Nat Comm	Exome.Ag
MEITL-15	17	40359729	T	G	missense_variant	17q21	STAT5B	NM_012448.3	c.1924A>C (p.Asn642His)	85.25%	62X	Nat Comm	Exome.Ag
MEITL-15	3	47147518	TGGATGT	T	disruptive_inframe_deletion	3p21	SETD2	NM_014159.6	c.4793_4807del (p.Arg1598_Ile1602del)	32%	227X	Nat Comm	Exome.Ag
MEITL-16	19	17948006	G	A	missense_variant	19p13	JAK3	NM_000215.3	c.1718C>T (p.Ala573Val)	35%	701X	NGSIyT	none
MEITL-16	19	17949121	T	G	missense_variant	19p13	JAK3	NM_000215.3	c.1520A>C (p.Gln507Pro)	42%	308X	NGSIyT	none
MEITL-16	3	47155365	C	A	splice_donor_variant&intron_variant	3p21	SETD2	NM_014159.6	c.4715+1G>T	30%	318X	NGSIyT	none
MEITL-16	3	47164495	G	T	stop_gained	3p21	SETD2	NM_014159.6	c.1631C>A (p.Ser544*)	19%	64X	NGSIyT	none
MEITL-17	1	65306942	G	A	missense_variant	1p31	JAK1	NM_002227.3	c.2635C>T (p.Arg879Cys)	10.93%	377X	Nat Comm	Exome.Ag
MEITL-17	17	40359729	T	G	missense_variant	17q21	STAT5B	NM_012448.3	c.1924A>C (p.Asn642His)	91.3%	70X	Nat Comm	Exome.Ag
MEITL-17	19	17945970	G	A	missense_variant	19p13	JAK3	NM_000215.3	c.1969C>T (p.Arg657Trp)	38.89%	91X	Nat Comm	Exome.Ag
MEITL-17	3	47058637	GTACT	G	frameshift_variant	3p21	SETD2	NM_014159.6	c.7637_7640del (p.Lys2546Thrfs*17)	32.67%	300X	Nat Comm	Exome.Ag
MEITL-17	3	47125468	AG	A	frameshift_variant	3p21	SETD2	NM_014159.6	c.5801del (p.Pro1934Leufs*11)	38.72%	359X	Nat Comm	Exome.Ag
MEITL-19	17	40359678	G	A	missense_variant	17q21	STAT5B	NM_012448.3	c.1975C>T (p.Arg659Cys)	2%	1482X	NGSIyT	none
MEITL-19	17	40359729	T	G	missense_variant	17q21	STAT5B	NM_012448.3	c.1924A>C (p.Asn642His)	26%	1302X	NGSIyT	none
MEITL-19	19	17948006	G	A	missense_variant	19p13	JAK3	NM_000215.3	c.1718C>T (p.Ala573Val)	4%	1122X	NGSIyT	none
MEITL-19	3	47059132	C	G	missense_variant	3p21	SETD2	NM_014159.6	c.7529G>C (p.Arg2510Pro)	55%	1025X	NGSIyT	none
MEITL-2	12	49441785	C	T	missense_variant	12q13	KMT2D	NM_003482.3	c.4199G>A (p.Cys1400Tyr)	42.05%	289X	Nat Comm	Exome.Ag
MEITL-2	17	7577538	C	T	missense_variant	17p13	TP53	NM_000546.5	c.743G>A (p.Arg248Gln)	91.47%	129X	Nat Comm	Exome.Ag
MEITL-2	3	47058746	T	G	splice_acceptor_variant&intron_variant	3p21	SETD2	NM_014159.6	c.7534-2A>C	40.82%	302X	Nat Comm	Exome.Ag
MEITL-2	3	47155483	C	T	missense_variant	3p21	SETD2	NM_014159.6	c.4598G>A (p.Cys1533Tyr)	41.98%	541X	Nat Comm	Exome.Ag
MEITL-20	17	40359729	T	G	missense_variant	17q21	STAT5B	NM_012448.3	c.1924A>C (p.Asn642His)	49.12%	116X	Nat Comm	Exome.Ag
MEITL-20	19	17948006	G	A	missense_variant	19p13	JAK3	NM_000215.3	c.1718C>T (p.Ala573Val)	51.72%	29X	Nat Comm	Exome.Ag
MEITL-20	3	47164398	TGTACAA	T	frameshift_variant	3p21	SETD2	NM_014159.6	c.1718_1727del (p.Phe573*)	40.51%	158X	Nat Comm	Exome.Ag
MEITL-20	3	47205343	C	T	splice_donor_variant&intron_variant	3p21	SETD2	NM_014159.6	c.71+1G>A	30.65%	63X	Nat Comm	Exome.Ag
MEITL-203	1	9780849	A	C	missense_variant	1p36	PIK3CD	NM_005026.3	c.1571A>C (p.Tyr524Ser)	32%	2011X	NGSIyT	none
MEITL-203	2	25462086	T	A	splice_acceptor_variant&intron_variant	2p23	DNMT3A	NM_022552.4	c.2323-2A>T	46%	1310X	NGSIyT	none
MEITL-203	3	47165110	A	C	stop_gained	3p21	SETD2	NM_014159.6	c.1016T>G (p.Leu339*)	34%	3978X	NGSIyT	none
MEITL-203	3	47165722	G	C	stop_gained	3p21	SETD2	NM_014159.6	c.404C>G (p.Ser135*)	31%	3570X	NGSIyT	none
MEITL-21	17	7578283	G	T	missense_variant	17p13	TP53	NM_000546.5	c.566C>A (p.Ala189Asp)	62.28%	294X	Nat Comm	Exome.Ag
MEITL-21	19	17948745	ATGCAGT	A	disruptive_inframe_deletion	19p13	JAK3	NM_000215.3	c.1688_1696del (p.Lys563_Cys565del)	24.4%	503X	Nat Comm	Exome.Ag
MEITL-21	3	47059204	A	C	missense_variant	3p21	SETD2	NM_014159.6	c.7457T>G (p.Leu2486Arg)	24.31%	144X	Nat Comm	Exome.Ag
MEITL-21	3	47098908	C	CCGGCTGTG	frameshift_variant	3p21	SETD2	NM_014159.6	c.6365_6366insTTGTGCCAGGACACAGCCG (p.	12.14%	384X	Nat Comm	Exome.Ag
MEITL-22	1	27089473	C	CCAGG	frameshift_variant	1p36	ARID1A	NM_006015.4	c.2433_2436dup (p.Pro813Alafs*5)	29.76%	84X	Nat Comm	Exome.Ag
MEITL-22	17	40354460	A	T	missense_variant	17q21	STAT5B	NM_012448.3	c.2135T>A (p.Val712Glu)	75.44%	57X	Nat Comm	Exome.Ag
MEITL-22	19	17949108	C	T	missense_variant	19p13	JAK3	NM_000215.3	c.1533G>A (p.Met511Ile)	27.78%	90X	Nat Comm	Exome.Ag
MEITL-22	3	47098913	G	GTTCTCCTTA	stop_gained&conservative_inframe_insertion	3p21	SETD2	NM_014159.6	c.6360_6361insTAAGGAGAA (p.Glu2120_Arg	21.88%	359X	Nat Comm	Exome.Ag
MEITL-22	3	47147591	A	T	missense_variant	3p21	SETD2	NM_014159.6	c.4735T>A (p.Tyr1579Asn)	32.37%	210X	Nat Comm	Exome.Ag

MEITL-23	17	40354787	T	A	nonsynonymous SNV	17q21.2	STAT5B	NM_012448.3	c.2117A>T (p.Gln706Leu)	95.61%	569X	Nat Comm	Exome.IDT
MEITL-23	19	17948006	G	A	missense_variant	19p13	JAK3	NM_000215.3	c.1718C>T (p.Ala573Val)	51.61%	155X	Nat Comm	Exome.IDT
MEITL-23	3	47058649	G	T	stopgain	3p21.31	SETD2	NM_014159.6	c.7629C>A (p.Tyr2543*)	75.41%	306X	Nat Comm	Exome.IDT
MEITL-23	3	47164727	T	A	stop_gained	3p21	SETD2	NM_014159.6	c.1399A>T (p.Lys467*)	21.54%	65X	Nat Comm	Exome.IDT
MEITL-24	17	40359729	T	G	missense_variant	17q21	STAT5B	NM_012448.3	c.1924A>C (p.Asn642His)	70.11%	87X	Nat Comm	Exome.Ag
MEITL-24	17	40359746	T	G	missense_variant&splice_region_variant	17q21	STAT5B	NM_012448.3	c.1907A>C (p.Gln636Pro)	60.94%	64X	Nat Comm	Exome.Ag
MEITL-24	17	7578530	A	G	missense_variant	17p13	TP53	NM_000546.5	c.400T>C (p.Phe134Leu)	79.22%	235X	Nat Comm	Exome.Ag
MEITL-24	3	47163203	C	A	stop_gained	3p21	SETD2	NM_014159.6	c.2923G>T (p.Gly975*)	28.76%	388X	Nat Comm	Exome.Ag
MEITL-24	X	41206209	AGAAAAC	A	conservative_inframe_deletion	Xp11	DDX3X	NM_001356.4	c.1717_1731del (p.Asn573_Glu577del)	56.03%	117X	Nat Comm	Exome.Ag
MEITL-24	X	41206236	C	G	stop_gained	Xp11	DDX3X	NM_001356.4	c.1740C>G (p.Tyr580*)	53.96%	139X	Nat Comm	Exome.Ag
MEITL-25	1	65307176	A	C	missense_variant	1p31	JAK1	NM_002227.3	c.2512T>G (p.Phe838Val)	43.05%	153X	Nat Comm	Exome.Ag
MEITL-25	17	40354460	A	T	missense_variant	17q21	STAT5B	NM_012448.3	c.2135T>A (p.Val712Glu)	81.82%	22X	Nat Comm	Exome.Ag
MEITL-25	3	47058649	G	C	stop_gained	3p21	SETD2	NM_014159.6	c.7629C>G (p.Tyr2543*)	40.59%	553X	Nat Comm	Exome.Ag
MEITL-25	3	47164536	AC	A	frameshift_variant	3p21	SETD2	NM_014159.6	c.1589del (p.Cys530Phefs*49)	41.52%	461X	Nat Comm	Exome.Ag
MEITL-26	17	40354787	T	A	missense_variant	17q21	STAT5B	NM_012448.3	c.2117A>T (p.Gln706Leu)	88.89%	73X	Nat Comm	Exome.Ag
MEITL-26	17	40362213	T	A	missense_variant	17q21	STAT5B	NM_012448.3	c.1882A>T (p.Thr628Ser)	93%	202X	Nat Comm	Exome.Ag
MEITL-26	3	47084126	G	GT	frameshift_variant	3p21	SETD2	NM_014159.6	c.7162dup (p.Thr2388Asnfs*41)	37.09%	304X	Nat Comm	Exome.Ag
MEITL-26	3	47144882	G	C	missense_variant	3p21	SETD2	NM_014159.6	c.4871C>G (p.Ser1624Cys)	47.3%	316X	Nat Comm	Exome.Ag
MEITL-27	19	17948006	G	A	missense_variant	19p13	JAK3	NM_000215.3	c.1718C>T (p.Ala573Val)	21%	281X	NGSIyT; Nat Comm	none
MEITL-27	20	39794862	A	G	missense_variant	20q12	PLCG1	NM_002660.2	c.1828A>G (p.Ile610Val)	22%	211X	NGSIyT; Nat Comm	none
MEITL-27	20	39802391	A	G	missense_variant	20q12	PLCG1	NM_002660.2	c.3494A>G (p.Asp1165Gly)	29%	86X	NGSIyT; Nat Comm	none
MEITL-27	3	47162268	A	C	stopgain	3p21.31	SETD2	NM_014159.6	c.3858T>G (p.Tyr1286*)	37.25%	102X	NGSIyT; Nat Comm	none
MEITL-28	17	40359729	T	G	missense_variant	17q21	STAT5B	NM_012448.3	c.1924A>C (p.Asn642His)	58.39%	149X	Nat Comm	Exome.IDT
MEITL-28	17	7577120	C	T	missense_variant	17p13	TP53	NM_000546.5	c.818G>A (p.Arg273His)	79.65%	231X	Nat Comm	Exome.IDT
MEITL-28	19	17948006	G	A	missense_variant	19p13	JAK3	NM_000215.3	c.1718C>T (p.Ala573Val)	50.72%	69X	Nat Comm	Exome.IDT
MEITL-3	3	47103835	TGCTAAG(	T	frameshift_variant&splice_acceptor_variant&splice_region_va	3p21	SETD2	NM_014159.6	c.6110-8_6110del (p.?)	16.14%	256X	Nat Comm	Exome.Ag
MEITL-3	X	39933279	TG	T	frameshift_variant	Xp11	BCOR	NM_001123383.1	c.1319del (p.Pro440Hisfs*2)	58.11%	224X	Nat Comm	Exome.Ag
MEITL-30	17	40354787	T	A	missense_variant	17q21	STAT5B	NM_012448.3	c.2117A>T (p.Gln706Leu)	72.9%	679X	NGSIyT; V1	Exome.IDT
MEITL-30	19	17945918	A	G	missense_variant	19p13	JAK3	NM_000215.3	c.2021T>C (p.Val674Ala)	35.98%	353X	NGSIyT; V1	Exome.IDT
MEITL-30	3	47129722	C	A	stop_gained	3p21	SETD2	NM_014159.6	c.5158G>T (p.Glu1720*)	47.42%	97X	NGSIyT; V1	Exome.IDT
MEITL-31	17	7578406	C	T	missense_variant	17p13	TP53	NM_000546.5	c.524G>A (p.Arg175His)	67.36%	144X	NGSIyT; V1	Exome.IDT
MEITL-31	19	17948006	G	A	missense_variant	19p13	JAK3	NM_000215.3	c.1718C>T (p.Ala573Val)	39.68%	126X	NGSIyT; V1	Exome.IDT
MEITL-31	3	47103828	G	A	stop_gained	3p21	SETD2	NM_014159.6	c.6118C>T (p.Arg2040*)	33.86%	127X	NGSIyT; V1	Exome.IDT
MEITL-33	17	40359729	T	G	missense_variant	17q21	STAT5B	NM_012448.3	c.1924A>C (p.Asn642His)	85%	565X	NGSIyT; V1	none
MEITL-33	2	20459167	G	A	missense_variant	2q33	CD28	NM_006139.3	c.376G>A (p.Glu126Lys)	43.6%	78X	NGSIyT; V1	none
MEITL-33	3	47165765	CA	C	frameshift_variant	3p21	SETD2	NM_014159.6	c.360del (p.Ile120Metfs*32)	80%	348X	NGSIyT; V1	none
MEITL-33	4	106156872	G	C	missense_variant	4q24	TET2	NM_001127208.2	c.1773G>C (p.Gln591His)	17.6%	255X	NGSIyT; V1	none
MEITL-34	1	9775768	G	A	missense_variant	1p36	PIK3CD	NM_005026.3	c.311G>A (p.Arg104His)	7.59%	79X	none	Exome.IDT
MEITL-34	1	9777666	C	A	missense_variant	1p36	PIK3CD	NM_005026.3	c.1002C>A (p.Asn334Lys)	12.4%	121X	none	Exome.IDT
MEITL-34	11	108175403	T	G	missense_variant&splice_region_variant	11q22	ATM	NM_000051.3	c.5498T>G (p.Val1833Gly)	28.09%	89X	none	Exome.IDT
MEITL-34	17	40359729	T	G	missense_variant	17q21	STAT5B	NM_012448.3	c.1924A>C (p.Asn642His)	80.66%	183X	none	Exome.IDT
MEITL-34	3	47058743	A	C	missense_variant&splice_region_variant	3p21	SETD2	NM_014159.6	c.7535T>G (p.Leu2512Arg)	37.93%	116X	none	Exome.IDT
MEITL-34	3	47162211	G	C	stop_gained	3p21	SETD2	NM_014159.6	c.3915C>G (p.Tyr1305*)	35.77%	137X	none	Exome.IDT
MEITL-35	19	17947967	A	T	missense_variant	19p13	JAK3	NM_000215.3	c.1757T>A (p.Leu586Gln)	36.24%	149X	none	Exome.IDT
MEITL-35	3	47084145	AG	A	frameshift_variant	3p21	SETD2	NM_014159.6	c.7143del (p.Ser2382Leufs*29)	33.48%	221X	none	Exome.IDT
MEITL-36	17	40359729	T	G	missense_variant	17q21	STAT5B	NM_012448.3	c.1924A>C (p.Asn642His)	90%	2396X	NGSIyT	none
MEITL-36	3	47161887	ACTCT	A	frameshift_variant	3p21	SETD2	NM_014159.6	c.4235_4238del (p.Glu1412Valfs*19)	39%	3583X	NGSIyT	none
MEITL-36	3	47165557	G	GGAGAT	frameshift_variant	3p21	SETD2	NM_014159.6	c.564_568dup (p.Pro190Hisfs*21)	38%	3816X	NGSIyT	none
MEITL-37	17	40359729	T	G	missense_variant	17q21	STAT5B	NM_012448.3	c.1924A>C (p.Asn642His)	96.88%	512X	V1	Exome.IDT
MEITL-37	17	7577539	G	A	missense_variant	17p13	TP53	NM_000546.5	c.742C>T (p.Arg248Trp)	86.73%	98X	V1	Exome.IDT
MEITL-37	19	17948006	G	A	missense_variant	19p13	JAK3	NM_000215.3	c.1718C>T (p.Ala573Val)	45%	100X	V1	Exome.IDT
MEITL-37	3	47127738	A	G	missense_variant	3p21	SETD2	NM_014159.6	c.5344T>C (p.Trp1782Arg)	97.04%	371X	V1	Exome.IDT
MEITL-37	3	50293704	C	T	missense_variant	3p21	GNAI2	NM_002070.3	c.545C>T (p.Thr182Ile)	40.48%	126X	V1	Exome.IDT
MEITL-38	1	65313304	C	A	missense_variant	1p31	JAK1	NM_002227.3	c.1810G>T (p.Asp604Tyr)	47.06%	204X	V1	Exome.IDT
MEITL-38	19	17948006	G	A	missense_variant	19p13	JAK3	NM_000215.3	c.1718C>T (p.Ala573Val)	90.91%	99X	V1	Exome.IDT
MEITL-38	3	47147591	A	T	missense_variant	3p21	SETD2	NM_014159.6	c.4735T>A (p.Tyr1579Asn)	93.94%	99X	V1	Exome.IDT
MEITL-39	17	40359729	T	G	missense_variant	17q21	STAT5B	NM_012448.3	c.1924A>C (p.Asn642His)	26.71%	161X	V1	Exome.IDT
MEITL-39	19	17948009	G	A	missense_variant	19p13	JAK3	NM_000215.3	c.1715C>T (p.Ala572Val)	69.84%	65X	V1	Exome.IDT
MEITL-39	3	47125871	A	T	missense_variant&splice_region_variant	3p21	SETD2	NM_014159.6	c.5399T>A (p.Ile1800Asn)	80.95%	42X	V1	Exome.IDT
MEITL-4	17	7578260	C	T	missense_variant	17p13	TP53	NM_000546.5	c.589G>A (p.Val197Met)	85.71%	126X	Nat Comm	Exome.Ag
MEITL-4	19	17948006	G	A	missense_variant	19p13	JAK3	NM_000215.3	c.1718C>T (p.Ala573Val)	54.17%	50X	Nat Comm	Exome.Ag
MEITL-4	3	47108557	T	A	splice_donor_variant&splice_region_variant&intron_variant	3p21	SETD2	NM_014159.6	c.6109+3A>T	85.37%	41X	Nat Comm	Exome.Ag
MEITL-40	17	40354460	A	T	missense_variant	17q21	STAT5B	NM_012448.3	c.2135T>A (p.Val712Glu)	77.4%	177X	V1	Exome.IDT
MEITL-40	17	40359746	T	C	missense_variant&splice_region_variant	17q21	STAT5B	NM_012448.3	c.1907A>G (p.Gln636Arg)	39.61%	154X	V1	Exome.IDT
MEITL-40	17	7577574	T	C	missense_variant	17p13	TP53	NM_000546.5	c.707A>G (p.Tyr236Cys)	72.13%	61X	V1	Exome.IDT
MEITL-40	3	47058661	TTTGTGTT	T	disruptive_inframe_deletion	3p21	SETD2	NM_014159.6	c.7604_7616delinsT (p.Asn2535_Lys2539deli	25%	192X	V1	Exome.IDT
MEITL-40	3	47155365	C	G	splice_donor_variant&intron_variant	3p21	SETD2	NM_014159.6	c.4715+1G>C	25.71%	140X	V1	Exome.IDT
MEITL-41	19	17948745	ATGCAGT	A	disruptive_inframe_deletion	19p13	JAK3	NM_000215.3	c.1688_1696del (p.Lys563_Cys565del)	7.88%	203X	V1	Exome.IDT
MEITL-41	3	47143034	G	C	missense_variant	3p21	SETD2	NM_014159.6	c.4929C>G (p.Asn1643Lys)	16.84%	95X	V1	Exome.IDT
MEITL-41	3	50293694	C	T	missense_variant	3p21	GNAI2	NM_002070.3	c.535C>T (p.Arg179Cys)	15.38%	78X	V1	Exome.IDT
MEITL-41	4	106157275	C	T	stop_gained	4q24	TET2	NM_001127208.2	c.2176C>T (p.Gln726*)	5.88%	255X	V1	Exome.IDT

MEITL-42	17	40359729	T	G	missense_variant	17q21	STAT5B	NM_012448.3	c.1924A>C (p.Asn642His)	100%	86X	none	Exome.IDT
MEITL-42	3	47058705	TAC	T	frameshift_variant	3p21	SETD2	NM_014159.6	c.7571_7572del (p.Cys2524*)	37.96%	108X	none	Exome.IDT
MEITL-42	3	47084050	C	A	splice_donor_variant&intron_variant	3p21	SETD2	NM_014159.6	c.7238+1G>T	36.21%	116X	none	Exome.IDT
MEITL-43	12	49420670	G	A	stop_gained	12q13	KMT2D	NM_003482.3	c.15079C>T (p.Arg5027*)	29%	2614X	NGSIyT	none
MEITL-43	17	40376874	G	A	missense_variant	17q21	STAT5B	NM_012448.3	c.298C>T (p.Arg100Cys)	17%	1524X	NGSIyT	none
MEITL-43	17	7577539	G	A	missense_variant	17p13	TP53	NM_000546.5	c.742C>T (p.Arg248Trp)	84%	1018X	NGSIyT	none
MEITL-43	19	17949108	C	T	missense_variant	19p13	JAK3	NM_000215.3	c.1533G>A (p.Met511Ile)	58%	2493X	NGSIyT	none
MEITL-43	3	47142943	C	A	splice_donor_variant&splice_region_variant&intron_variant	3p21	SETD2	NM_014159.6	c.5015+5G>T	43%	1169X	NGSIyT	none
MEITL-43	3	47162045	G	A	stop_gained	3p21	SETD2	NM_014159.6	c.4081C>T (p.Gln1361*)	39%	2221X	NGSIyT	none
MEITL-44	12	49431762	C	A	missense_variant	12q13	KMT2D	NM_003482.3	c.9377G>T (p.Gly3126Val)	49%	1756X	NGSIyT; V1	none
MEITL-44	16	24135155	G	A	splice_acceptor_variant&intron_variant	16p12	PRKCB	NM_002738.6	c.919-1G>A	36%	2340X	NGSIyT; V1	none
MEITL-44	3	47125235	A	G	missense_variant	3p21	SETD2	NM_014159.6	c.6035T>C (p.Leu2012Pro)	31%	2699X	NGSIyT; V1	none
MEITL-45	11	10820102[illegible]	T	C	missense_variant	11q22	ATM	NM_000051.3	c.7390T>C (p.Cys2464Arg)	49%	1405X	V2	none
MEITL-45	17	40359729	T	G	missense_variant	17q21	STAT5B	NM_012448.3	c.1924A>C (p.Asn642His)	42%	1396X	V2	none
MEITL-45	19	17949108	C	A	missense_variant	19p13	JAK3	NM_000215.3	c.1533G>T (p.Met511Ile)	34%	732X	V2	none
MEITL-45	20	39791914	G	T	missense_variant&splice_region_variant	20q12	PLCG1	NM_002660.2	c.788G>T (p.Gly263Val)	49%	524X	V2	none
MEITL-45	3	47163347	C	A	stop_gained	3p21	SETD2	NM_014159.6	c.2779G>T (p.Glu927*)	29%	1763X	V2	none
MEITL-45	7	2946316	C	T	missense_variant	7p22	CARD11	NM_032415.5	c.3421G>A (p.Glu1141Lys)	49%	553X	V2	none
MEITL-46	1	65325801	G	A	missense_variant	1p31	JAK1	NM_002227.3	c.1321C>T (p.His441Tyr)	38.56%	153X	NGSIyT	Exome.IDT
MEITL-46	19	17948006	G	A	missense_variant	19p13	JAK3	NM_000215.3	c.1718C>T (p.Ala573Val)	46.48%	71X	NGSIyT	Exome.IDT
MEITL-46	3	47127758	C	T	missense_variant	3p21	SETD2	NM_014159.6	c.5324G>A (p.Gly1775Glu)	10%	1646X	NGSIyT	Exome.IDT
MEITL-46	3	47142981	T	A	missense_variant	3p21	SETD2	NM_014159.6	c.4982A>T (p.Glu1661Val)	73.61%	72X	NGSIyT	Exome.IDT
MEITL-47	1	65305427	T	C	missense_variant	1p31	JAK1	NM_002227.3	c.2701A>G (p.Thr901Ala)	37%	1567X	NGSIyT	none
MEITL-47	19	17949108	C	G	missense_variant	19p13	JAK3	NM_000215.3	c.1533G>C (p.Met511Ile)	36%	1369X	NGSIyT	none
MEITL-47	3	47164596	A	T	stop_gained	3p21	SETD2	NM_014159.6	c.1530T>A (p.Tyr510*)	43%	1650X	NGSIyT	none
MEITL-47	3	47165661	T	TGG	frameshift_variant	3p21	SETD2	NM_014159.6	c.463_464dup (p.Leu156Hisfs*9)	36%	1771X	NGSIyT	none
MEITL-47	4	10618292[illegible]	CTG	C	frameshift_variant	4q24	TET2	NM_001127208.2	c.3965_3966del (p.Leu1322Argfs*16)	2%	1595X	NGSIyT	none
MEITL-49	11	10820227[illegible]	G	A	missense_variant	11q22	ATM	NM_000051.3	c.7618G>A (p.Val2540Ile)	50.54%	279X	none	Exome.IDT
MEITL-49	17	40354460	A	T	missense_variant	17q21	STAT5B	NM_012448.3	c.2135T>A (p.Val712Glu)	91.19%	227X	none	Exome.IDT
MEITL-49	17	7574017	C	A	missense_variant	17p13	TP53	NM_000546.5	c.1010G>T (p.Arg337Leu)	81%	100X	none	Exome.IDT
MEITL-49	19	17949108	C	T	missense_variant	19p13	JAK3	NM_000215.3	c.1533G>A (p.Met511Ile)	53.65%	274X	none	Exome.IDT
MEITL-49	2	25457290	C	T	splice_acceptor_variant&intron_variant	2p23	DNMT3A	NM_022552.4	c.2598-1G>A	41.15%	192X	none	Exome.IDT
MEITL-5	17	7578271	T	C	missense_variant	17p13	TP53	NM_000546.5	c.578A>G (p.His193Arg)	54%	337X	NGSIyT; Nat Comm	none
MEITL-5	3	47084145	A	AG	frameshift_variant	3p21	SETD2	NM_014159.6	c.7143dup (p.Ser2382Leufs*47)	35%	1528X	NGSIyT; Nat Comm	none
MEITL-5	3	47088067	A	AAT	frameshift_variant	3p21	SETD2	NM_014159.6	c.7006_7007dup (p.Thr2338Serfs*16)	30%	1654X	NGSIyT; Nat Comm	none
MEITL-50	19	17948745	ATGCAGT	A	disruptive_inframe_deletion	19p13	JAK3	NM_000215.3	c.1688_1696del (p.Lys563_Cys565del)	43.98%	166X	none	Exome.IDT
MEITL-50	3	47059132	C	G	missense_variant	3p21	SETD2	NM_014159.6	c.7529G>C (p.Arg2510Pro)	37.1%	62X	none	Exome.IDT
MEITL-50	3	47144849	C	A	missense_variant	3p21	SETD2	NM_014159.6	c.4904G>T (p.Cys1635Phe)	33.33%	101X	none	Exome.IDT
MEITL-51	19	17949121	T	G	missense_variant	19p13	JAK3	NM_000215.3	c.1520A>C (p.Gln507Pro)	30.36%	112X	none	Exome.IDT
MEITL-52	17	40359659	T	A	missense_variant	17q21	STAT5B	NM_012448.3	c.1994A>T (p.Tyr665Phe)	58.56%	333X	none	Exome.IDT
MEITL-52	19	17948006	G	A	missense_variant	19p13	JAK3	NM_000215.3	c.1718C>T (p.Ala573Val)	45.45%	77X	none	Exome.IDT
MEITL-52	3	47161913	T	A	stop_gained	3p21	SETD2	NM_014159.6	c.4213A>T (p.Lys1405*)	47.46%	118X	none	Exome.IDT
MEITL-53	17	40359729	T	G	missense_variant	17q21	STAT5B	NM_012448.3	c.1924A>C (p.Asn642His)	81.62%	185X	none	Exome.IDT
MEITL-53	19	17948006	G	A	missense_variant	19p13	JAK3	NM_000215.3	c.1718C>T (p.Ala573Val)	34.18%	79X	none	Exome.IDT
MEITL-53	3	47059133	G	C	missense_variant	3p21	SETD2	NM_014159.6	c.7528C>G (p.Arg2510Gly)	40.48%	126X	none	Exome.IDT
MEITL-53	3	47147534	G	A	stop_gained	3p21	SETD2	NM_014159.6	c.4792C>T (p.Arg1598*)	35.62%	146X	none	Exome.IDT
MEITL-54	17	40359729	T	G	missense_variant	17q21	STAT5B	NM_012448.3	c.1924A>C (p.Asn642His)	89.89%	178X	none	Exome.IDT
MEITL-54	3	47165608	A	T	stop_gained	3p21	SETD2	NM_014159.6	c.518T>A (p.Leu173*)	91.4%	221X	none	Exome.IDT
MEITL-55	17	7578402	GC	G	frameshift_variant	17p13	TP53	NM_000546.5	c.527del (p.Cys176Serfs*71)	81%	1444X	NGSIyT	none
MEITL-55	3	47155464	A	C	missense_variant	3p21	SETD2	NM_014159.6	c.4617T>G (p.Cys1539Trp)	43%	3881X	NGSIyT	none
MEITL-55	3	47165741	C	A	stop_gained	3p21	SETD2	NM_014159.6	c.385G>T (p.Glu129*)	44%	3783X	NGSIyT	none
MEITL-56	17	40359729	T	G	missense_variant	17q21	STAT5B	NM_012448.3	c.1924A>C (p.Asn642His)	83%	765X	NGSIyT	none
MEITL-56	17	7577538	C	T	missense_variant	17p13	TP53	NM_000546.5	c.743G>A (p.Arg248Gln)	81%	817X	NGSIyT	none
MEITL-56	3	47098304	TAGTTA	T	splice_donor_variant&splice_region_variant&intron_variant	3p21	SETD2	NM_014159.6	c.6963+2_6963+6del	16%	846X	NGSIyT	none
MEITL-56	3	47163533	TA	T	frameshift_variant	3p21	SETD2	NM_014159.6	c.2592del (p.Asn865Ilefs*26)	39%	1895X	NGSIyT	none
MEITL-57	17	7577526	A	G	missense_variant	17p13	TP53	NM_000546.5	c.755T>C (p.Leu252Pro)	66%	818X	NGSIyT	none
MEITL-57	19	17955108	C	T	missense_variant	19p13	JAK3	NM_000215.3	c.119G>A (p.Arg40His)	49%	2612X	NGSIyT	none
MEITL-57	3	47058734	C	CCTGTAGT	frameshift_variant	3p21	SETD2	NM_014159.6	c.7541_7543delinsCCGACTACAG (p.His2514P	47%	1984X	NGSIyT	none
MEITL-58	17	40359729	T	G	missense_variant	17q21	STAT5B	NM_012448.3	c.1924A>C (p.Asn642His)	47%	2059X	NGSIyT; V1	none
MEITL-58	19	17948006	G	A	missense_variant	19p13	JAK3	NM_000215.3	c.1718C>T (p.Ala573Val)	41%	1434X	NGSIyT; V1	none
MEITL-58	3	47165024	G	A	stop_gained	3p21	SETD2	NM_014159.6	c.1102C>T (p.Arg368*)	40%	3102X	NGSIyT; V1	none
MEITL-58	4	10619403[illegible]	C	T	missense_variant	4q24	TET2	NM_001127208.2	c.4492C>T (p.Arg1498Cys)	46%	2951X	NGSIyT; V1	none
MEITL-59	17	40364159	C	T	missense_variant	17q21	STAT5B	NM_012448.3	c.1523G>A (p.Cys508Tyr)	45%	2389X	NGSIyT	none
MEITL-59	17	7578406	C	T	missense_variant	17p13	TP53	NM_000546.5	c.524G>A (p.Arg175His)	49%	2011X	NGSIyT	none
MEITL-59	3	47098421	G	A	stop_gained	3p21	SETD2	NM_014159.6	c.6853C>T (p.Gln2285*)	28%	2839X	NGSIyT	none
MEITL-59	3	47125799	A	C	missense_variant	3p21	SETD2	NM_014159.6	c.5471T>G (p.Ile1824Ser)	13%	2665X	NGSIyT	none
MEITL-59	3	47165261	C	T	missense_variant	3p21	SETD2	NM_014159.6	c.865G>A (p.Asp289Asn)	5%	2588X	NGSIyT	none

MEITL-6	1	65309803	G	A	missense_variant	1p31	JAK1	NM_002227.3	c.2347C>T (p.Leu783Phe)	15.31%	522X	Nat Comm	Exome.IDT
MEITL-6	1	65312365	A	G	missense_variant	1p31	JAK1	NM_002227.3	c.1954T>C (p.Tyr652His)	8.97%	301X	Nat Comm	Exome.IDT
MEITL-6	17	7579362	A	C	missense_variant	17p13	TP53	NM_000546.5	c.325T>G (p.Phe109Val)	87.54%	321X	Nat Comm	Exome.IDT
MEITL-6	19	17949108	C	T	missense_variant	19p13	JAK3	NM_000215.3	c.1533G>A (p.Met511Ile)	55.73%	314X	Nat Comm	Exome.IDT
MEITL-62	17	7577121	G	A	missense_variant	17p13	TP53	NM_000546.5	c.817C>T (p.Arg273Cys)	19%	1898X	NGSlyT	none
MEITL-62	17	7579356	G	T	missense_variant	17p13	TP53	NM_000546.5	c.331C>A (p.Leu111Met)	22%	1672X	NGSlyT	none
MEITL-62	19	17947968	G	C	missense_variant	19p13	JAK3	NM_000215.3	c.1756C>G (p.Leu586Val)	27%	1126X	NGSlyT	none
MEITL-62	3	47098450	G	C	stop_gained	3p21	SETD2	NM_014159.6	c.6824C>G (p.Ser2275*)	21%	3483X	NGSlyT	none
MEITL-63	1	65305421	C	T	missense_variant	1p31	JAK1	NM_002227.3	c.2707G>A (p.Glu903Lys)	40%	2717X	NGSlyT	none
MEITL-63	17	7577547	C	T	missense_variant	17p13	TP53	NM_000546.5	c.734G>A (p.Gly245Asp)	82%	911X	NGSlyT	none
MEITL-63	19	17949121	T	G	missense_variant	19p13	JAK3	NM_000215.3	c.1520A>C (p.Gln507Pro)	85%	2760X	NGSlyT	none
MEITL-63	3	47098937	G	GGC	frameshift_variant	3p21	SETD2	NM_014159.6	c.6336_6337insGC (p.Arg2113Alafs*35)	36%	2652X	NGSlyT	none
MEITL-63	3	47142980	C	G	missense_variant	3p21	SETD2	NM_014159.6	c.4983G>C (p.Glu1661Asp)	38%	2269X	NGSlyT	none
MEITL-63	X	39934182	TC	T	frameshift_variant	Xp11	BCOR	NM_001123383.1	c.416del (p.Gly139Glufs*22)	63%	3629X	NGSlyT	none
MEITL-64	11	108196144	G	A	missense_variant	11q22	ATM	NM_000051.3	c.6680G>A (p.Arg2227His)	92%	1461X	NGSlyT	none
MEITL-64	3	47165583	TG	T	frameshift_variant	3p21	SETD2	NM_014159.6	c.542del (p.Thr181Lysfs*3)	37%	4236X	NGSlyT	none
MEITL-65	17	40359729	T	G	missense_variant	17q21	STAT5B	NM_012448.3	c.1924A>C (p.Asn642His)	53%	2012X	NGSlyT	none
MEITL-65	3	47079266	G	A	stop_gained&splice_region_variant	3p21	SETD2	NM_014159.6	c.7240C>T (p.Gln2414*)	38%	1719X	NGSlyT	none
MEITL-65	3	47165754	TA	T	frameshift_variant	3p21	SETD2	NM_014159.6	c.371del (p.Leu124Tyrfs*28)	43%	2494X	NGSlyT	none
MEITL-65	X	39922122	G	GT	frameshift_variant&stop_gained	Xp11	BCOR	NM_001123383.1	c.3947dup (p.Tyr1316*)	5%	2917X	NGSlyT	none
MEITL-66	17	40354460	A	T	missense_variant	17q21	STAT5B	NM_012448.3	c.2135T>A (p.Val712Glu)	54%	1111X	NGSlyT	none
MEITL-66	17	7578406	C	T	missense_variant	17p13	TP53	NM_000546.5	c.524G>A (p.Arg175His)	40%	1296X	NGSlyT	none
MEITL-66	3	47142993	G	A	missense_variant	3p21	SETD2	NM_014159.6	c.4970C>T (p.Pro1657Leu)	25%	1739X	NGSlyT	none
MEITL-67	12	49415848	C	T	missense_variant	12q13	KMT2D	NM_003482.3	c.16499G>A (p.Arg5500Gln)	25%	1310X	NGSlyT	none
MEITL-67	17	7577058	C	A	stop_gained	17p13	TP53	NM_000546.5	c.880G>T (p.Glu294*)	89%	1000X	NGSlyT	none
MEITL-67	3	47165338	A	C	stop_gained	3p21	SETD2	NM_014159.6	c.788T>G (p.Leu263*)	35%	374X	NGSlyT	none
MEITL-67	X	41200862	A	AG	frameshift_variant&splice_region_variant	Xp11	DDX3X	NM_001356.4	c.281dup (p.Arg95Lysfs*3)	91%	487X	NGSlyT	none
MEITL-7	17	40359729	T	G	nonsynonymous SNV	17q21.2	STAT5B	NM_012448.3	c.1924A>C (p.Asn642His)	49.34%	1279X	NGSlyT; Nat Comm	none
MEITL-7	17	40370341	T	C	missense_variant	17q21	STAT5B	NM_012448.3	c.997A>G (p.Ile333Val)	38%	1423X	NGSlyT; Nat Comm	none
MEITL-7	3	47088072	G	A	stop_gained	3p21	SETD2	NM_014159.6	c.7003C>T (p.Gln2335*)	44%	1779X	NGSlyT; Nat Comm	none
MEITL-7	3	47165267	CA	C	frameshift_variant	3p21	SETD2	NM_014159.6	c.858del (p.Ile286Metfs*15)	40%	992X	NGSlyT; Nat Comm	none
MEITL-70	17	40354460	A	T	missense_variant	17q21	STAT5B	NM_012448.3	c.2135T>A (p.Val712Glu)	55%	969X	NGSlyT	none
MEITL-70	3	47088036	G	A	stop_gained	3p21	SETD2	NM_014159.6	c.7039C>T (p.Gln2347*)	26%	2695X	NGSlyT	none
MEITL-70	X	39923699	C	A	missense_variant	Xp11	BCOR	NM_001123383.1	c.3392G>T (p.Arg1131Leu)	53%	2414X	NGSlyT	none
MEITL-71	17	7577131	G	C	missense_variant	17p13	TP53	NM_000546.5	c.807C>G (p.Ser269Arg)	55%	784X	NGSlyT	none
MEITL-71	3	47165204	TAG	T	frameshift_variant	3p21	SETD2	NM_014159.6	c.920_921del (p.Ser307*)	33%	1244X	NGSlyT	none
MEITL-73	11	108141988	T	C	missense_variant	11q22	ATM	NM_000051.3	c.2932T>C (p.Ser978Pro)	14%	1812X	NGSlyT	none
MEITL-73	11	108235824	C	A	missense_variant	11q22	ATM	NM_000051.3	c.8866C>A (p.Pro2956Thr)	35%	2602X	NGSlyT	none
MEITL-73	17	40359729	T	G	missense_variant	17q21	STAT5B	NM_012448.3	c.1924A>C (p.Asn642His)	11%	2901X	NGSlyT	none
MEITL-73	3	47164413	AT	A	frameshift_variant	3p21	SETD2	NM_014159.6	c.1712del (p.Asn571Ilefs*8)	37%	3369X	NGSlyT	none
MEITL-73	3				missense_variant;frameshift_variant	3p21	SETD2	NM_014159.6	c.[354G>A; 360_366del] (p.[Met118Ile; Gly12	34%; 30%	2832X; 2589X	NGSlyT	none
MEITL-74	1	65312365	A	G	missense_variant	1p31	JAK1	NM_002227.3	c.1954T>C (p.Tyr652His)	11%	2421X	NGSlyT	none
MEITL-74	17	40359729	T	G	missense_variant	17q21	STAT5B	NM_012448.3	c.1924A>C (p.Asn642His)	24%	2441X	NGSlyT	none
MEITL-74	3	47161887	ACTCT	A	frameshift_variant	3p21	SETD2	NM_014159.6	c.4235_4238del (p.Glu1412Valfs*19)	12%	3963X	NGSlyT	none
MEITL-74	3	47165734	GA	G	frameshift_variant	3p21	SETD2	NM_014159.6	c.391del (p.Ser131Profs*21)	12%	3621X	NGSlyT	none
MEITL-74	7	2978338	C	T	missense_variant	7p22	CARD11	NM_032415.5	c.992G>A (p.Arg331His)	46%	1765X	NGSlyT	none
MEITL-74	X	39931909	G	A	missense_variant	Xp11	BCOR	NM_001123383.1	c.2690C>T (p.Ser897Leu)	47%	2641X	NGSlyT	none
MEITL-74	X	39932689	G	C	missense_variant	Xp11	BCOR	NM_001123383.1	c.1910C>G (p.Ser637Cys)	47%	2642X	NGSlyT	none
MEITL-9	11	108124663	A	G	missense_variant	11q22	ATM	NM_000051.3	c.2021A>G (p.His674Arg)	46%	399X	NGSlyT; Nat Comm	none
MEITL-9	11	108160506	T	G	missense_variant	11q22	ATM	NM_000051.3	c.4414T>G (p.Leu1472Val)	46%	312X	NGSlyT; Nat Comm	none
MEITL-9	17	40354460	A	T	missense_variant	17q21	STAT5B	NM_012448.3	c.2135T>A (p.Val712Glu)	37%	190X	NGSlyT; Nat Comm	none
MEITL-9	17	40359729	T	G	missense_variant	17q21	STAT5B	NM_012448.3	c.1924A>C (p.Asn642His)	32%	351X	NGSlyT; Nat Comm	none
MEITL-9	3	47147507	T	C	missense_variant	3p21	SETD2	NM_014159.6	c.4819A>G (p.Met1607Val)	60%	230X	NGSlyT; Nat Comm	none
MEITL-202	3	47139440	C	T	splicing_variant		SETD2	NM_014159.6	c.5142+5G>A	9.4%	395X	V1	none

‡ Panel legend

Nat Comm : TDS with 9 genes (*CREBB, JAK1, JAK2, JAK3, SETD2, STAT5B, STAT1, STAT3, STAT5A*) used in the Nature communication publication of Roberti et al. 2016 (1).
V1 : TDS with 9 genes (*CD28, DNMT3A, IDH2, PLCG1, RHOA, SETD2, STAT3, STAT5B, TET2,*) as previously described[4.]

NGSlyT: TDS with 27 genes (*ARID1A, ATM, BCOR, CARD11, CCR4, CD28, CTNNB1, DDX3X, DNMT3A, FYN, IDH2, IRF4, JAK1, JAK3, KMT2D, PIK3CD, PLCG1, PRKCB, RHOA, SETD2, SOCS1, STAT3, STAT5B, TET2, TNFRSF1B, TP53, VAV1*) as described in "Material and Methods" of the main manuscript.

Exome.IDT : Whole exome sequencing perfromed with IDT probes as described in "Material and Methods" of the main manuscript

Exome.Ag: Whole exome sequencing perfromed with Agilent probes and used in the Nature communication publication of Roberti et al. 2016[1.]

Supplementary Table S6. Univariate analysis of overall survival in MEITL (n=63).

Characteristics	n (%)	median OS	*P*	HR	CI
Age (years)					
<70	38 (60.3%)	9.7	**0.039**	1.75	1.03-2.98
≥70	25 (39.7%)	3.3.			
Gender					
Male	31 (49.2%)	8.4	0.788	1.07	0.64-1.82
Female	32 (50.8%)	5.8			
Bowel perforation					
No	17 (27.9%)	10.8	0.484	1.24	0.68-2.28
Yes	44 (72.1%)	5.8			
Surgical procedure					
Anastomosis	24 (61.5%)	10.3	**0.015**	2.43	1.19-4.97
Enterostomy	15 (38.5%)	5.2			
PS					
0-2	42 (75%)	10.8	**<0.005**	4.46	2.15-9.28
3-4	14 (25%)	3.9			
Lugano stage					
1	21 (35%)	17.3	**0.025**	1.96	1.09-3.54
≥2	39 (65%)	5.7			
Response to first-line chemotherapy					
CR	15 (35.7%)	21.1	**<0.005**	5.85	2.66-12.88
non-CR	27 (64.3%)	7.9			
Cytology					
Monomorphic	47 (74.6%)	10.3	**0.013**	2.12	1.17-3.85
Non-monomorphic	16 (25.4%)	4.3			
Necrosis					
No	54 (85.7%)	7.9	0.61	1.2	0.59-2.46
Yes	9 (14.3%)	5.2			
Starry-sky/apoptosis					
No	56 (88.9%)	8.3	0.27	1.6	0.68-3.76
Yes	7 (11.1%)	1.1			
Angiotropism/angioinvasion					
No	41 (71.9%)	9.7	**0.034**	1.9	1.05-3.57
Yes	16 (28.1%)	5.2			
Atypical histology					
No	36 (57.1%)	10.8	**0.011**	2.00	1.17-3.41
Yes	27 (42.9%)	5.2			
Ki-67					
≤50%	18 (29.5%)	7.9	0.809	1.08	0.59-1.96
>50%	43 (70.5%)	5.8			
CD56					
Negative	7 (11.1%)	3.4	0.208	0.60	0.27-1.33
Positive	56 (88.9%)	7.9			
TCR β					
Negative	40 (70.2%)	7.9	0.290	1.38	0.76-2.52

Positive	17 (29.8%)	5.6			
TCRγδ					
Negative	28 (50%)	7.9	0.575	1.17	0.67-2.05
Positive	28 (50%)	5.2			
TCR expression status					
Silent	15 (27.8%)	7.9	0.594	1.20	0.62-2.31
Expressed	39 (72.2%)	5.6			
B-cell marker expression					
Negative	48 (77.4%)	7.8	**0.046**	0.49	0.24-0.99
Positive	14 (22.6%)	12.4			
MYC expression (IHC)					
No (<25%)	34 (68%)	9.7	**0.005**	2.56	1.33-4.95
Yes (25-100%)	16 (32%)	3.4			
***MYC* gene (FISH)**					
Normal FISH pattern	46 (82.1%)	7.9	0.150	1.72	0.82-3.59
Copy gain or rearrangement	10 (17.9%)	3.4			
H3K36 trimethylation					
Normal	5 (8.5%)	10.3	0.558	0.76	0.30-1.92
Defective	54 (91.5%)	5.8			
p53 expression (IHC)					
Wild type pattern	35 (67.3%)	9.5	0.244	1.44	0.78-2.66
Mutated pattern	17 (32.7%)	5.6			
***TP53* mutation**					
No	38 (66.7%)	9.7	**0.016**	2.11	1.15-3.87
Yes	19 (33.3%)	5.6			
***STAT5B* mutation**					
No	22 (38.6%)	10.3	0.101	1.6	0.91-2.90
Yes	35 (61.4%)	4.3			
***TP53/STAT5B* mutation(s)**					
Both wild-type	13 (22.8%)	13.7			
TP53 or *STAT5B* mutation	35 (61.4%)	5.6	**0.058**	2.00	0.98-4.12
TP53 and *STAT5B* mutations	9 (15.8%)	1.8	**0.007**	3.54	1.41-8.87
***JAK3* mutation**					
No	30 (53.6%)	5.6	0.303	0.74	0.42-1.31
Yes	26 (46.4%)	5.8			
***JAK1* mutation**					
No	50 (89.3%)	5.7	0.293	1.60	0.67-3.82
Yes	6 (10.7%)	2.9			
***ATM* mutation**					
No	49 (89.1%)	5.7	0.660	0.81	0.32-2.06
Yes	6 (10.9%)	1.1			
***BCOR* mutation**					
No	47 (87%)	5.6	0.534	1.30	0.57-2.93
Yes	7 (13%)	9.7			
***SETD2* mutation**					
Yes	51 (89.5%)	1.1	0.150	1.9	0.79-4.47
No	6 (10.5%)	7.9			

Abbreviations: CR, complete response; PS, Performance Status; FISH, fluorescent in situ hybridization; IHC, immunohistochemistry.

Estimates of overall survival were constructed using the Kaplan-Meier method. Cox proportional hazards regression model was used to investigate associated prognostic factors in univariate analysis. Results were expressed as hazard-ratio (HR) and 95% confidence interval. Statistical analysis was performed using Stata software. The tests were two-sided, with a type I error set at 5%. A Sidak's type I error correction was applied to consider multiple comparisons.

Supplementary Table S7. Detailed multivariable analysis.

	Multivariable analyses						***Sensitivity analysis***		
N=44	***Final model analysis***			***Bootstrap analysis***					
	HR	**95% CI**	***P value***	**HR**	**95% CI**	***P value***	**HR**	**95% CI**	***P value***
B-cell marker expression	0.15	0.05 – 0.46	0.001	0.15	0.03 – 0.85	0.032	0.15	0.04 – 0.55	0.004
***TP53* mutation**	4.86	1.75 – 13.5	0.002	4.86	1.25 – 18.9	0.022	4.85	1.73 – 13.6	0.003
***STAT5B* mutation**	3.42	1.44 – 8.13	0.005	3.42	1.03 – 11.4	0.045	3.40	1.40 – 8.26	0.007
MYC expression (IHC)	3.06	1.33 – 7.04	0.009	3.06	1.02 – 9.2	0.046	3.07	1.30 – 7.27	0.011
Performance Status ≥2	6.46	2.44 – 17.1	<0.001	6.46	2.06 – 20.2	0.001	6.64	2.41 – 18.2	<0.001
Age ≥70	NA	NA	NA	NA	NA	NA	0.98	0.43 – 2.20	0.953
Lugano stage ≥2	NA	NA	NA	NA	NA	NA	1.08	0.44 – 2.65	0.865

NA: not assessed.

Supplementary Table S8. Characteristics of long survivor patients

MEITL No	OS (months) ; status	Age	Clinical Presentation	Stage	Localizations	PS	Surgery	Treatment	Response	Relapse	Atypical histology	IHC	*MYC gene* alteration	*TP53 mutation*	*STAT5B mutation*	*SETD2 mutation*	Other mutations
41	29 ; Alive, CR	69	Occlusion	1	Small bowel, large bowel	1	+	CHOP	CR	-	-	CD2- CD4- CD8+ CD56+ TCR- CD20- CD79a- MYC- p53-	-	-	-	+	*JAK3 GNAI2 TET2*
69	32 ; Dead (disease)	66	Perforation	1	Small bowel	1	+	CHOP	CR	+	-	CD2- CD4- CD8+ CD56+ CD20- MYC-	ND	ND	ND	ND	ND
42	45, Alive, CR	63	Perforation	4	Small bowel, abdominal wall, pelvic tumor	1	+	CHOEP	CR	-	+	CD2+ CD4- CD8+ CD56+ TCRγδ CD20+ CD79a+ MYC- p53-	-	-	+	+	-
23	46 ; Dead (disease)	72	Perforation	4	Small bowel, abdominal wall, bladder	2	+	CHOP	PR	+	+	CD2- CD4- CD8+ CD56+ TCR- CD20- CD79a- MYC- p53+	-	-	+	+	*JAK3*
35	47 ; Alive, CR	68	Perforation	1	Small bowel, large bowel	1	+	CHOP	CR	-	-	CD2+ CD4+ CD8+ CD56+ TCRβ CD20+ CD79a- MYC- p53-	-	-	-	+	*JAK3*
34	55 ; Alive, CR	90	Perforation	1	Small bowel	1	+	-	CR	-	-	CD2+ CD4- CD8+ CD56+ TCRγδ CD20+ CD79a- MYC- p53-	-	-	+	+	*ATM PIK3CD*
27	69 ; Alive, CR	66	Perforation	4	Small bowel, lung, tongue	0	+	CHOP + IVE-MTX	CR	+	-	CD2+ CD4- CD8+ CD56+ CD20+ CD79a- MYC- p53-	ND	-	-	+	*JAK3 PLCG1*
30	71 ; Dead (disease)	46	ND	ND	ND	ND	+	ND	ND	+	-	CD2- CD4- CD8- CD56+ TCR- CD20- MYC- p53-	-	-	+	+	*JAK3*

Abbreviations: CHOP, Cyclophosphamide, Doxorubicin, Vincristine, Prednisone; CHOEP, Cyclophosphamide, Doxorubicin, Vincristine, Etoposide, Prednisone; CR, complete response; IVE-MTX, Ifosfamide, Epirubicin, Etoposide, Methotrexate; ND, no data; OS: overall survival; PR, partial response

Supplementary Figures

Supplementary Figure S1. Digital database designed to record the morphological features, immunohistochemical and FISH results of MEITL cases.

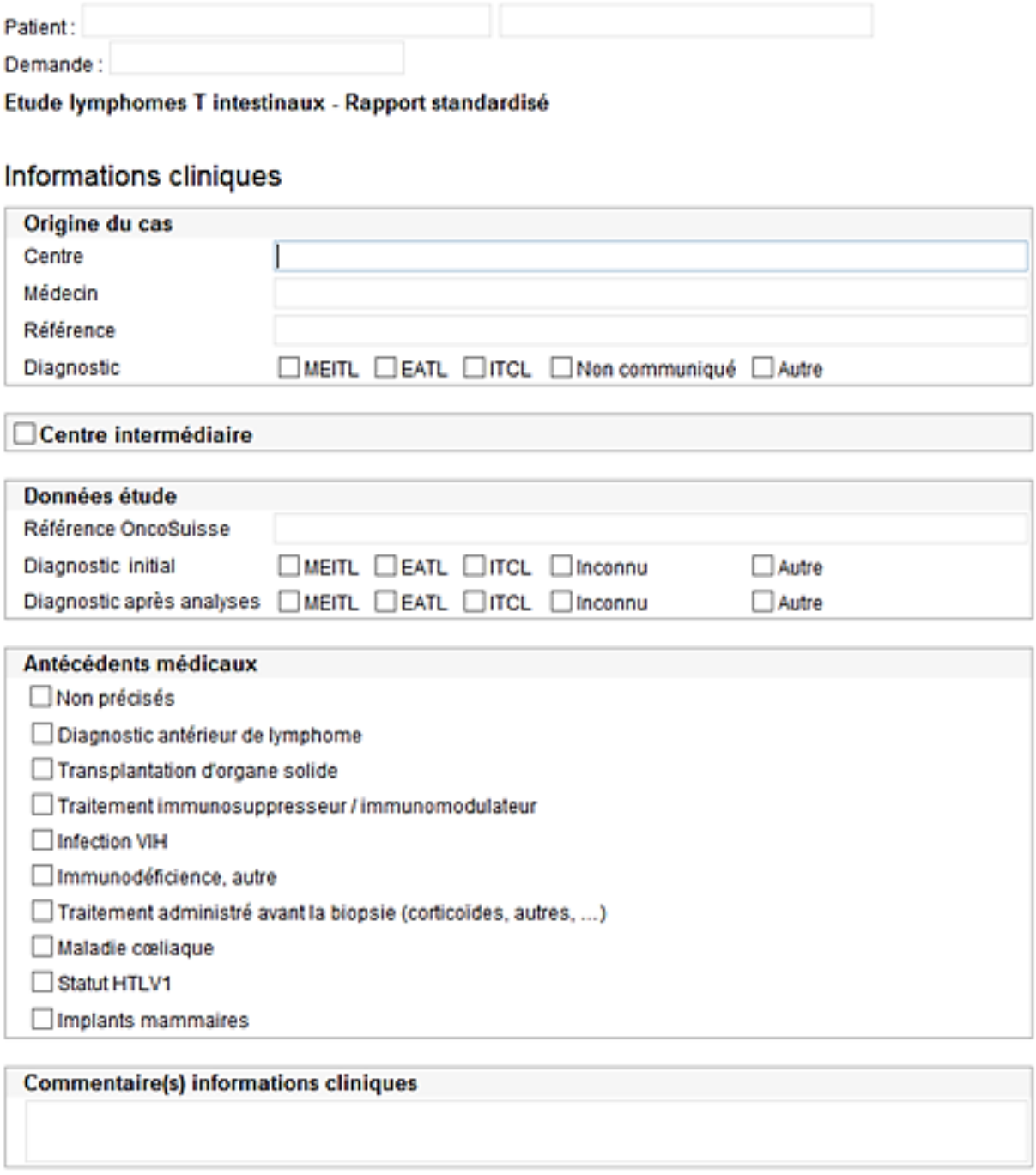
Patient :

Demande :

Etude lymphomes T intestinaux - Rapport standardisé

Informations cliniques

Origine du cas

Centre

Médecin

Référence

Diagnostic ☐ MEITL ☐ EATL ☐ ITCL ☐ Non communiqué ☐ Autre

☐ **Centre intermédiaire**

Données étude

Référence OncoSuisse

Diagnostic initial ☐ MEITL ☐ EATL ☐ ITCL ☐ Inconnu ☐ Autre

Diagnostic après analyses ☐ MEITL ☐ EATL ☐ ITCL ☐ Inconnu ☐ Autre

Antécédents médicaux

☐ Non précisés

☐ Diagnostic antérieur de lymphome

☐ Transplantation d'organe solide

☐ Traitement immunosuppresseur / immunomodulateur

☐ Infection VIH

☐ Immunodéficience, autre

☐ Traitement administré avant la biopsie (corticoïdes, autres, ...)

☐ Maladie cœliaque

☐ Statut HTLV1

☐ Implants mammaires

Commentaire(s) informations cliniques

Matériel

Description

Nombre de lames

Nombre de blocs

Ajouter un bloc ré-encodé

Examen macroscopique

Type de prélèvement

- [ ] Ganglion(s) lymphatique(s)
- [ ] Rate
- [ ] Médiastin
- [ ] Moelle osseuse
- [ ] Peau
- [ ] Organes digestifs (préciser)
- [ ] Epiploon
- [ ] Autre

Latéralité de l'échantillon

- ○ Non applicable
- ○ Non précisée
- ○ Gauche
- ○ Droite

Type de procédure

- ○ Biopsie chirurgicale
- ○ Biopsie à l'aiguille
- ○ Résection chirurgicale
- ○ Résection endoscopique
- ○ Ponction cytologique
- ○ Autre
- ○ Non précisé

Taille de la lésion

Taille (cm) Préciser ☐ Non communiquée

Commentaire(s) examen macroscopique

Examen microscopique

Tissu lésionnel

Infiltration

- ☐ Muqueuse
- ☐ Sous-muqueuse
- ☐ Musculeuse
- ☐ Tissu adipeux et/ou péritoine
- ☐ Autre

Perforation

- ○ Présente
- ○ Absente
- ○ Non évaluable
- ○ Autre

Ulcération

- ○ Présente
- ○ Absente
- ○ Non évaluable
- ○ Autre

Infiltration ganglionnaire

- ○ Présente
- ○ Absente
- ○ Non évaluable
- ○ Autre

Nécrose

Nécrose (%) Préciser

" Fat rimming "

- ○ Présent
- ○ Absent
- ○ Non évaluable
- ○ Autre

Cytologie & Patterns

Morphologie cellulaire	○ Monomorphe	○ Pléomorphe	○ Autre
Anaplasique	○ Absent	○ Minorité de cellules tumorales	○ Majorité de cellules tumorales
Blastoïde	○ Absent	○ Minorité de cellules tumorales	○ Majorité de cellules tumorales
"Starry sky"	○ Absent	○ Focal	○ Extensif

☐ Autre

Epithéliotropisme

- ○ Présent
- ○ Absent
- ○ Non évaluable
- ○ Autre

Angiotropisme

- ○ Présent
- ○ Absent
- ○ Non évaluable
- ○ Autre

Inflammation

Inflammation (%) Préciser

Commentaire Préciser

Taille cellulaire

- ☐ Petite
- ☐ Moyenne
- ☐ Grande
- ☐ Autre

Commentaire(s)

Paroi à distance

Entéropathie

- ○ Présente
- ○ Absente
- ○ Non évaluable

Lymphome intra-épithélial

- ○ Présent
- ○ Absent
- ○ Non évaluable

Marges de résection

- ○ Non applicable
- ○ RX: Ne peuvent être évaluées
- ○ R0: Marges exemptes de tumeur
- ○ R1: Marges positives microscopiques
- ○ R2: Marges positives macroscopiques

Autre(s) observation(s) microscopique(s)

- ☐ Hyperplasie lymphoïde
- ☐ Inflammation chronique
- ☐ Autre

Commentaire(s)

Immunophénotype / Biomarqueurs

Immunohistochimie

- ☐ Tumeur
- ☐ Lymphocytes intra-épithéliaux
- ☐ Lymphome intra-épithélial

Analyses génétiques / moléculaires

Analyses FISH

- ○ Non effectuée(s)
- ○ Effectuée(s)

Recherche de clonalité lymphoïde

- ○ Non effectuée
- ○ Effectuée

☐ Elément(s) d'intérêt didactique

Utilisation du cas

- ☐ TMA
- ☐ Séquençage DNA
- ☐ Méthylome
- ☐ RNAseq
- ☐ IEL à distance: cas éligible pour analyse(s)
- ☐ Autre

Commentaire(s)

Commentaire(s) supplémentaire(s)

Supplementary Figure S2. MEITL in non-intestinal organs. MEITL with anal involvement (MEITL 44, A-D), MEITL with lymph node involvement (MEITL 53, E-F) and massive involvement of the bone marrow (MEITL 16, G-H).

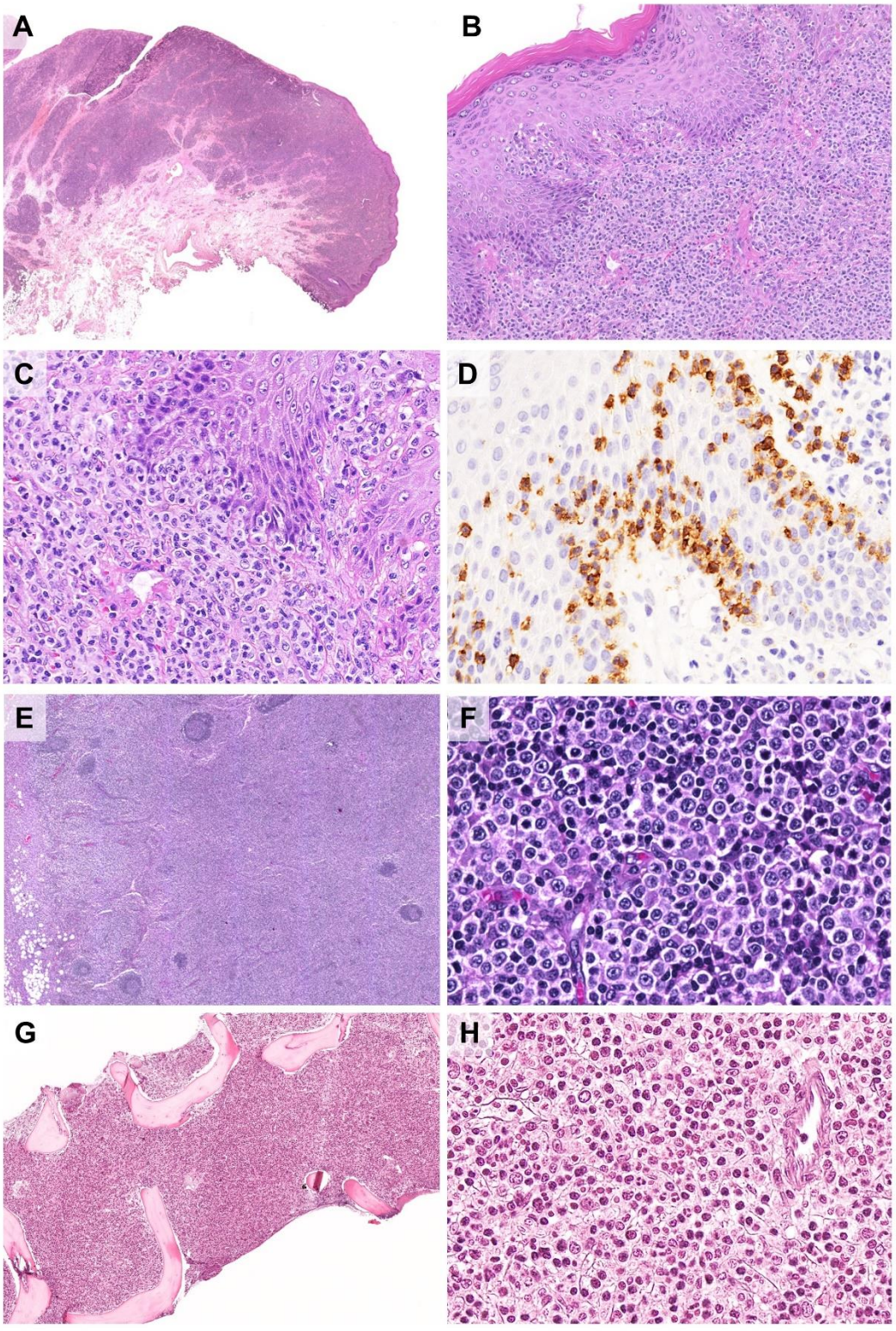

(A) This case shows a diffuse and dense infiltrate of tumor cells involving the entire thickness of the skin, and focally the subcutaneous fat, with surface ulceration. **(B** and **C)** Tumor cells show important epitheliotropism in the squamous epithelium of anal mucosa. **(D)** Epitheliotropic tumor cells are strongly positive for CD103. **(E)** Lymph node involved by MEITL shows a massive infiltration of paracortex with some residual B-cell follicles. **(F)** Tumor cells show a non-monomorphic cytology with intermediate/large sized tumor cells, many with evident nucleoli and ample cytoplasm. **(G)** This case shows a packed bone marrow with an extensive tumor infiltration. **(H)** Tumor cells display a monomorphic cytology. Original magnifications: x12.5 (A), x25 (E), x50 (G), x100 (B), x400 (C, D, F, H).

Supplementary Figure S3. MEITL with peculiar immunophenotypes (with B-cell antigen expression (case 42, A-C), with MYC expression (case 2, D-F) and double positive for TCR isoforms (case 56, G-I).

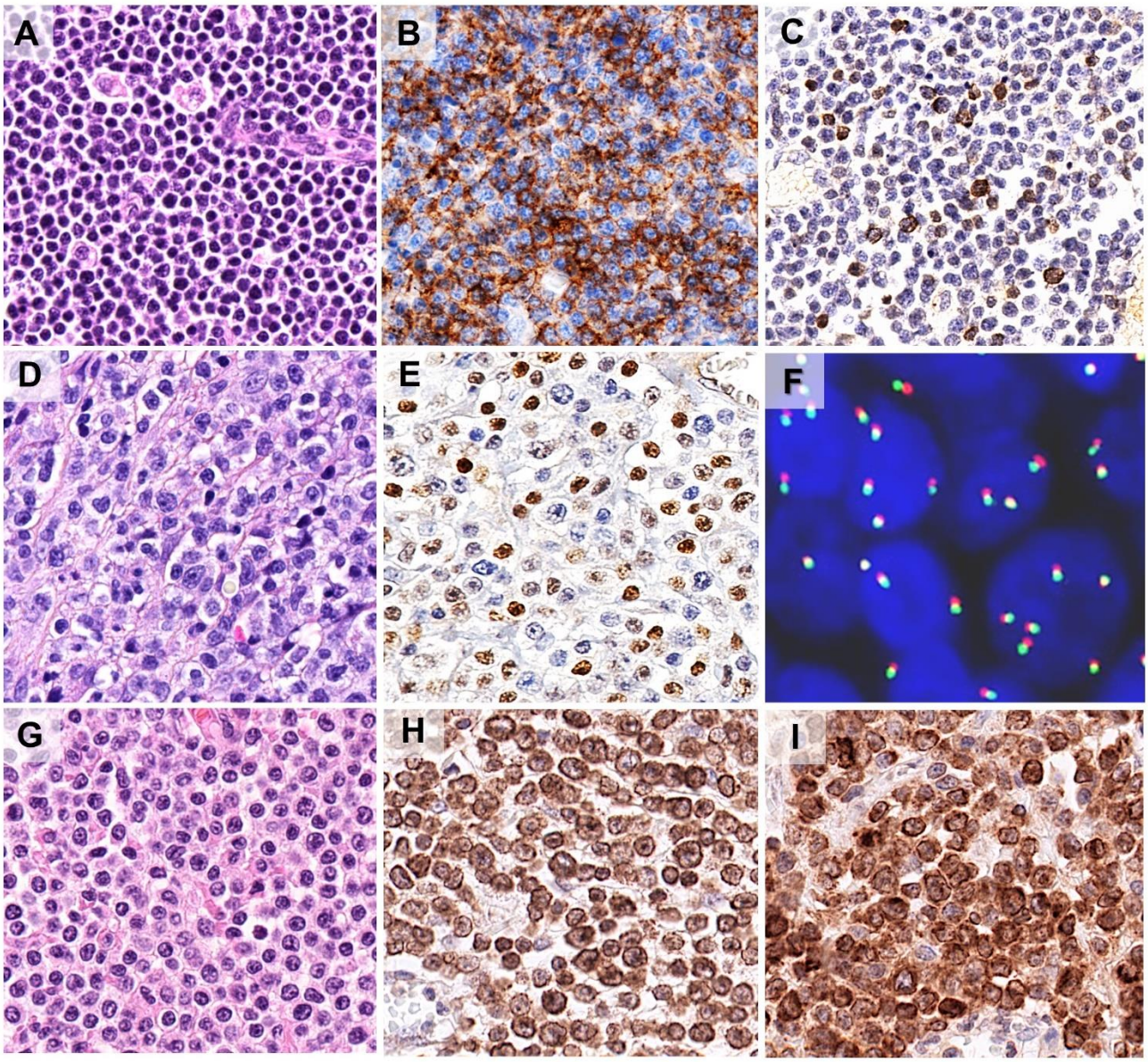

(A) This tumor shows an atypical “starry-sky” pattern. **(B)** Tumor cells are diffusely positivity for CD20. **(C)** CD79a is expressed in occasional atypical tumor cells. **(D)** Intermediate/large-sized tumor cells show nuclear pleomorphism and conspicuous nucleoli. **(E)** MYC was positive in most tumor cells. **(F)** *MYC* FISH shows many tumor cells with gene copy gains (3-6 signals/nucleus). **(G)** This tumor is composed of intermediate-sized tumor cells with clear cytoplasm and slight nuclear irregularity. **(H)** The

lymphoma cells were positive for TCRβ, and **(I)** TCRδ. Original magnifications: ×400 (A-E,G-I), x630 (F).

Supplementary Figure S4. Morphological, immunophenotypical and genetic characteristics of atypical MEITL case No. 66.

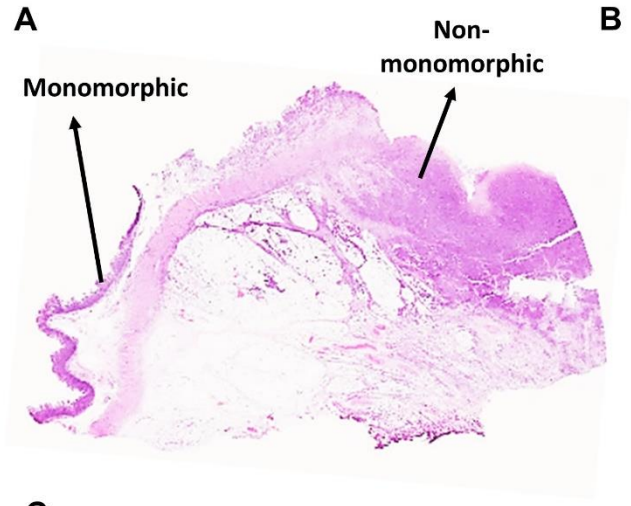

B

	Monomorphic	Non-monomorphic
IHC		
CD4	+	+
CD8	-	+
CD56	-	+
TIA1	-	+
Ki-67	15%	50%
CD30	<1%	~15%
Genetics		
STAT5B (p.Val712Glu) VAF	64	54
TP53 (p.Arg175His) VAF	45	40
SETD2 (p.Pro1657Leu) VAF	28	25
MYC FISH	Normal	Rearrangements (49%)

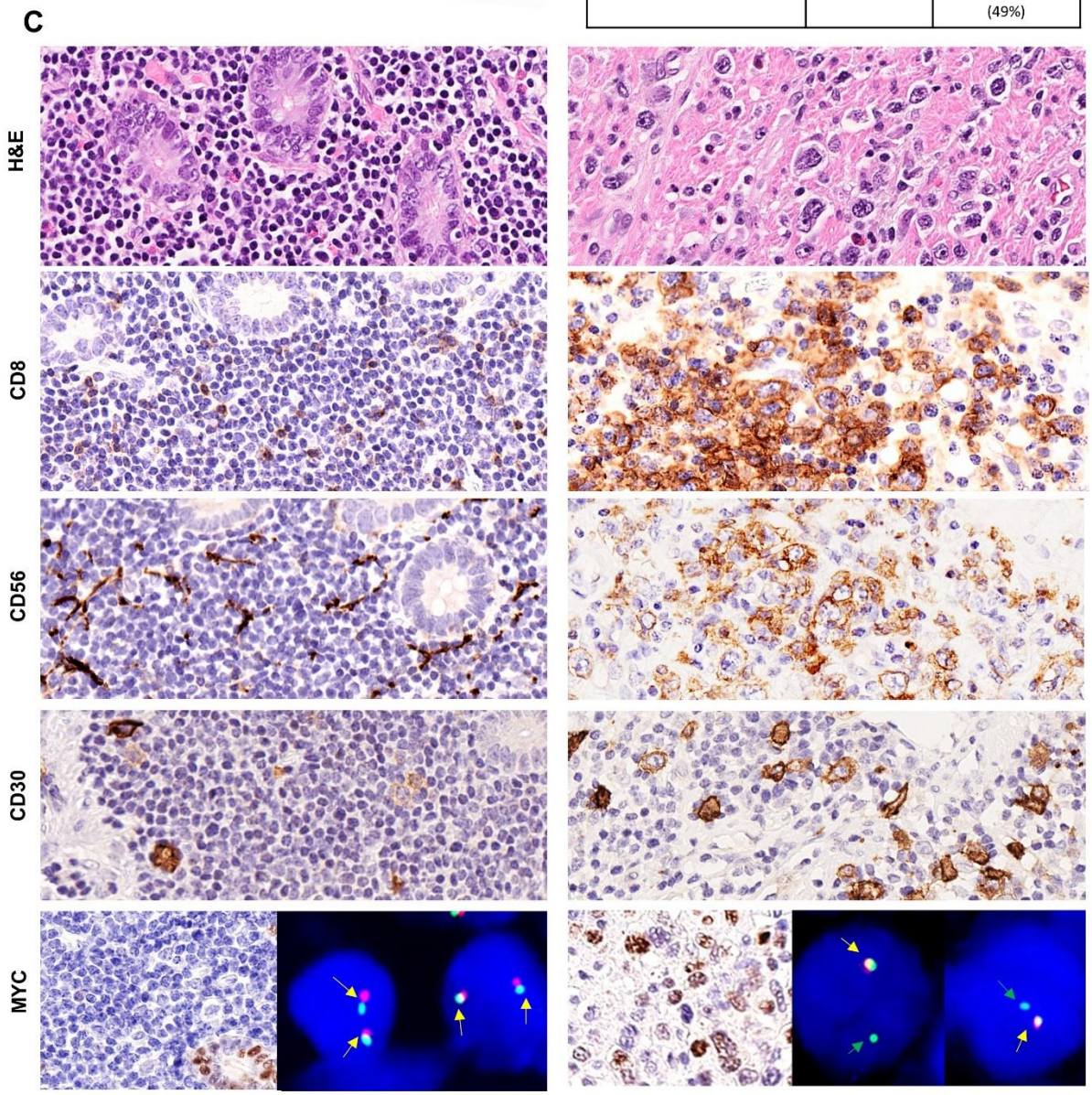

(A) This case shows two well-defined tumor areas: one corresponding to the intramucosal component of the peripheral zone, composed of small and round lymphocytes with a monomorphic cytology (left). The other area represents the central zone characterized by a non-monomorphic cytology with many large cells reminiscent of Hodgkin and Reed-Sternberg cells (right). **(B** and **C)** The two areas display distinctive immunophenotypic profiles: tumor cells with monomorphic cytology show an atypical immunophenotype: CD4+, CD8-, CD56-, TIA1-, are CD30- and show low proliferation (Ki-67~15%). In contrast, the non-monomorphic component is CD4+, CD8+, CD56+, TIA1+, CD30-/+ and display a higher proliferation (Ki-67 50%). Although cytologically and immunophenotypically different, which suggested initially the co-occurrence of two different types of T-cell lymphoma, an identical mutational profile (*SETD2, TP53* and *STAT5B* mutations at similar VAF) was observed, which confirmed the clonal relationship of both component and also diagnosis of MEITL in the two areas. Interestingly, *MYC* FISH study shows a pattern compatible with a gene rearrangement in the non-monomorphic component (49% of nuclei showed a loss of one red signal), which is associated with MYC overexpression (bottom right). On the contrary, *MYC* FISH study is normal in the monomorphic component, which is negative for MYC by immunohistochemistry (bottom left). Original magnifications: x400 (H&E, IHC in C), x630 (FISH in C).

Supplementary Figure S5. MEITL (#49) with preserved H3K36me3 trimethylation associated with the lack of *SETD2* gene alterations.

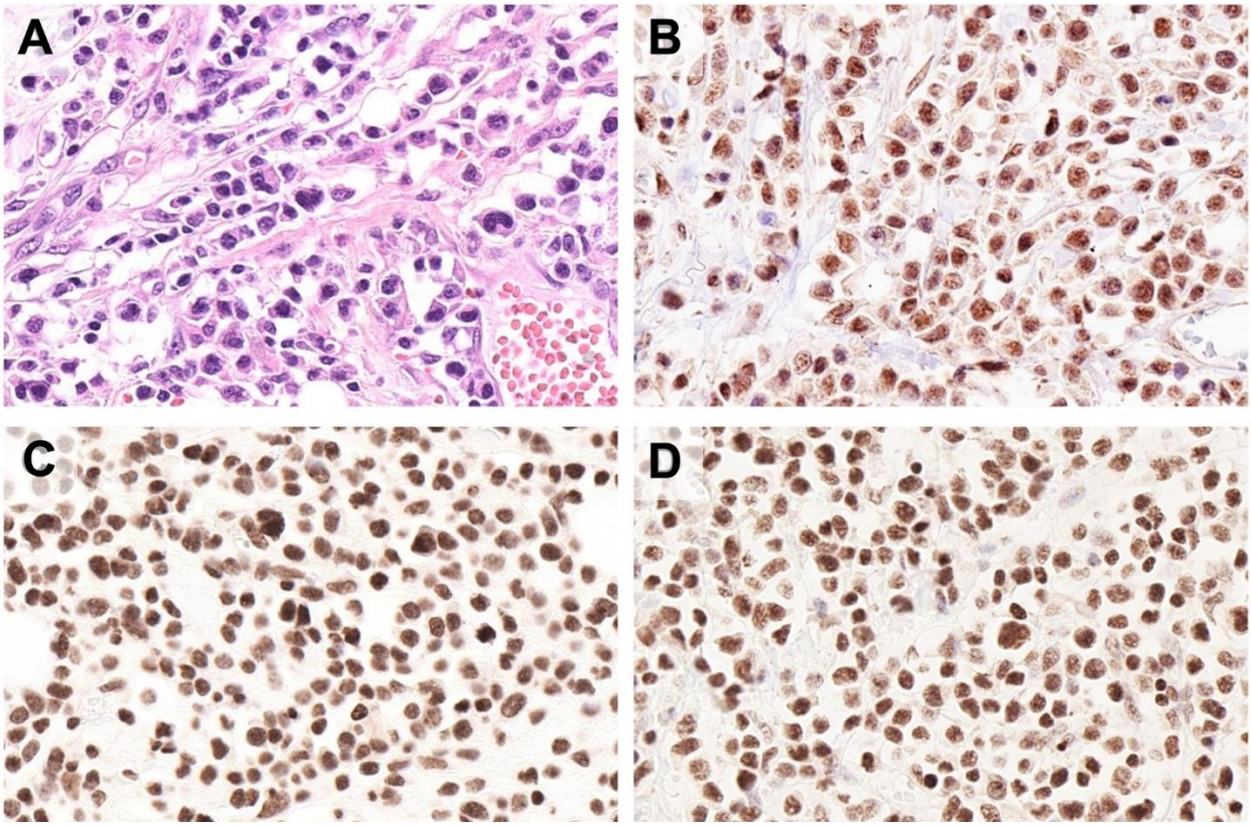

Exceptional case of MIETL with preserved H3K36me3 trimethylation. **(A)** The lymphoma cells show a non-monomorphic cytology, and **(B)** strong nuclear positivity for SETD2, and **(C)** H3K36me2, and **(D)** preserved expression of H3K36me3.

Supplementary Figure S6. Allele frequencies and loss of heterozygosity status observed for *JAK3*, *SETD2*, *STAT5B* and *TP53* mutations.

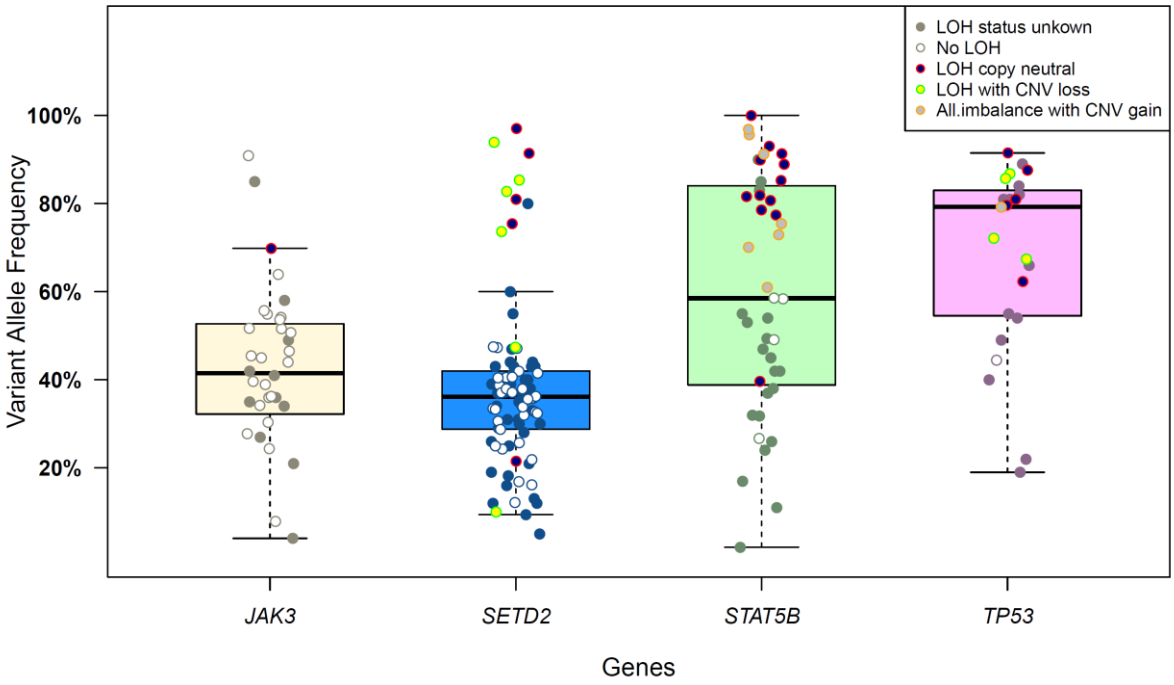

Box and whisker plot showing the distribution of allele frequencies observed for mutations in *JAK3*, *SETD2*, *STAT5B* and *TP53* genes. In addition, copy number variations as well as loss of heterozygosity (LOH) status were assessed from the 34 samples for which WES were performed. These co-occurring alterations were pointed in the plot with specific marks, as reported in the legend figure on the top right corner. Overall, of the 24 mutations observed in *STAT5B* by WES analysis, 23 (96%) had co-occurring LOH or allelic imbalance events (12 neutral, 7 with a CNV gain and 1 with CNV loss of the *STAT5B* locus) as previously observed (1). For *TP53*, out of the 11 mutations detected by WES, 10 (91%) were also associated with LOH (5 neutral, 4 with a CNV loss and 1 with CNV gain of the *TP53* locus). In comparison, *JAK3* (3/25 – 12%) and *SETD2* (12/45 – 27%) showed a significant lower number of LOH or allelic imbalance events associated with their mutations (for all comparison $p<0.001$, Fisher's exact test, while no statistical differences were observed between *STAT5B versus TP53* and *JAK3 versus SEDT2*). The

allele frequencies were also statistically significantly higher for mutations detected in *STAT5B* and *TP53* when compared with *SETD2* (both $p<0.001$, Wilcoxon rank sum test) and *JAK3* ($p<0.005$ and $p<0.001$, respectively). Again, no difference were observed between *STAT5B* and *TP53*, while a marginal higher allele frequencies was seen in *JAK3* versus *SEDT2* ($p=0.017$).

Supplementary Figure S7. Sankey plot of treatment and outcome of 63 MEITL patients

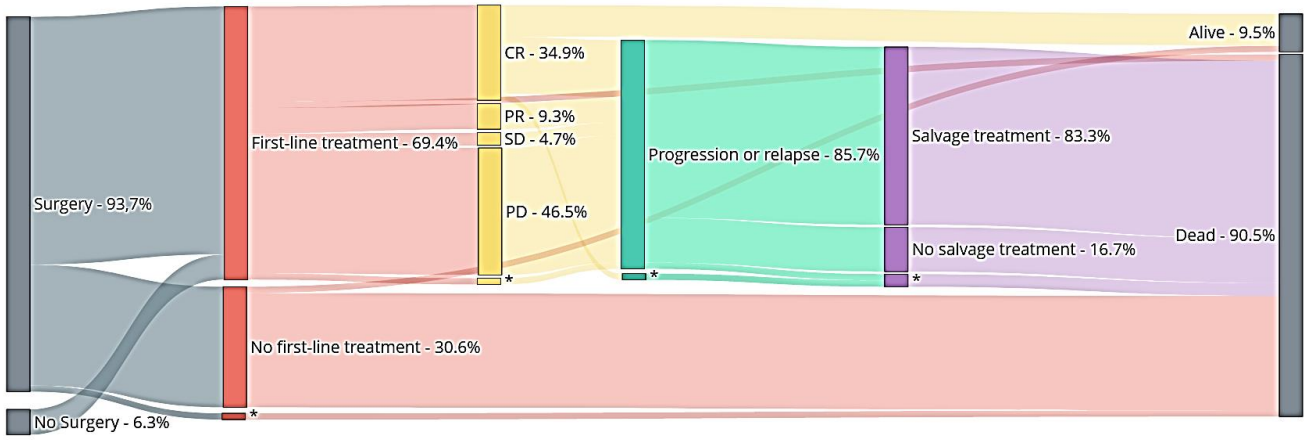

*Abbreviations: CR, complete remission; PR, partial response; SD, stable disease; PD, progressive disease, * unknown information.*

The height of flows is proportional to the number of patients. The length of flows is not proportional to time. Missing data/unknown information are not included in percentages. The median time between surgery and first-line treatment was 33 days with a range of 11 to 153 days. 57 patients died in a median time of 5.7 months (0-71 months), and 6 patients are alive and in complete remission at a median time of 45.8 months from diagnosis (5.6-69 months). The follow-up was 7.8 months for the whole cohort and 45.8 months in survivors. Abbreviations: CR, complete remission; PR, partial response; SD, stable disease; PD, progressive disease, * unknown information.

Supplementary Figure S8. Overall survival in MEITL according to treatment received and TCR expression.

A

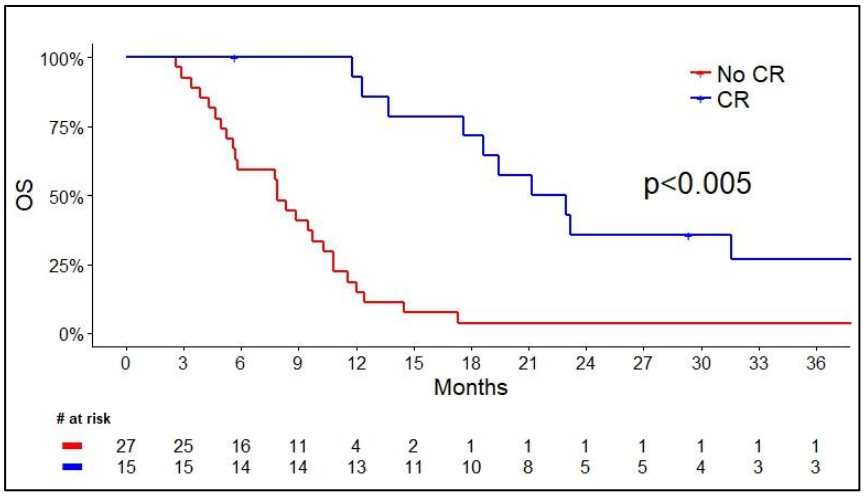

B

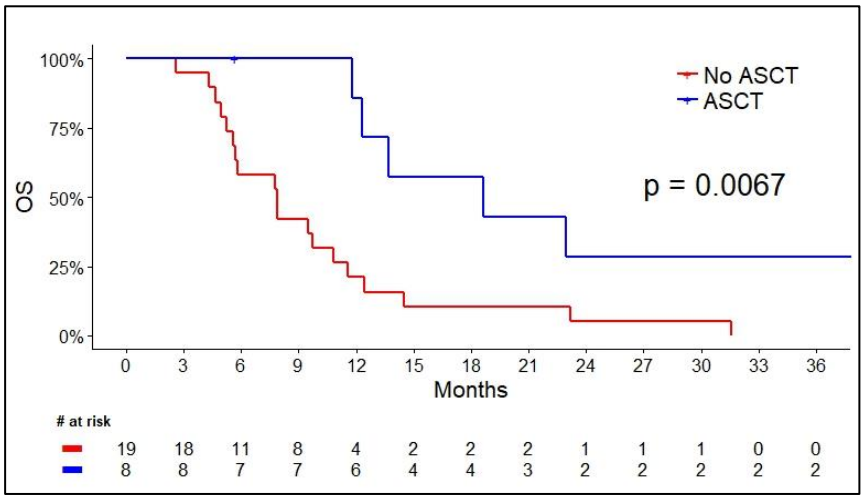

C

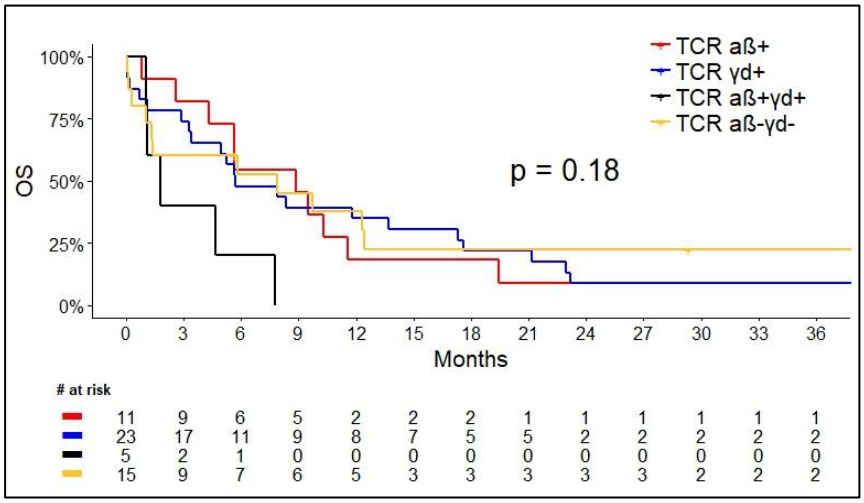

(A) Overall survival in months according to the response to first-line treatment, **(B)** according to ASCT in patients receiving a first-line treatment and younger than 67 years

old at diagnosis**,** and **(C)** according to the TCR expression. *Abbreviations: CR, complete response; OS, Overall Survival; ASCT, autologous stem cell transplantation*

References

1. Roberti A, Dobay MP, Bisig B, et al. Type II enteropathy-associated T-cell lymphoma features a unique genomic profile with highly recurrent SETD2 alterations. Nat commun. 2016;7:12602.

2. Trimech M, Letourneau A, Missiaglia E, et al. Angioimmunoblastic T-Cell Lymphoma and Chronic Lymphocytic Leukemia/Small Lymphocytic Lymphoma: A Novel Form of Composite Lymphoma Potentially Mimicking Richter Syndrome. Am J Surg Pathol. 2021;45(6):773-786.

3. Fajardo KF, Adams D, NISC Comparative Sequencing Program; Mason CE, Sincan M, Tifft C, et al. Detecting false-positive signals in exome sequencing. Hum Mutat. 2012;33(4):609-613.

4. Lemonnier F, Dupuis J, Sujobert P, et al. Treatment with 5-azacytidine induces a sustained response in patients with angioimmunoblastic T-cell lymphoma. Blood. 2018;132(21):2305-2309.